Topology optimization of damage-resistant structures with a predefined load-bearing capacity

Barbier, Tobias; Shakour, Emad; Sigmund, Ole; Lombaert, Geert; Schevenels, Mattias

Published in:
International Journal for Numerical Methods in Engineering

Link to article, DOI:
10.1002/nme.6891

Publication date:
2022

Document Version
Peer reviewed version

RESEARCH ARTICLE

Topology optimization of damage-resistant structures with a predefined load-bearing capacity

Tobias Barbier*[1] | Emad Shakour[2] | Ole Sigmund[3] | Geert Lombaert[4] | Mattias Schevenels[1]

[1]Faculty of Engineering Science, Department of Architecture, KU Leuven, Leuven, Belgium
[2]Faculty of Civil and Environmental Engineering, Technion – Israel Institute of Technology, Haifa, Israel
[3]Department of Mechanical Engineering, Solid Mechanics, Technical University of Denmark, Kongens Lyngby, Denmark
[4]Faculty of Engineering Science, Department of Civil Engineering, KU Leuven, Leuven, Belgium

Correspondence
*Tobias Barbier, Kasteelpark Arenberg 1 box 2431, 3001 Leuven, Belgium.
Email: tobias.barbier@kuleuven.be

Summary

This paper presents a novel strategy for structural topology optimization considering damage. In engineering practice, structures are typically designed to have a certain load-bearing capacity, with a minimal material volume or cost. We aim to optimize the topology of a structure to have a minimal weight while guaranteeing a predefined load capacity, considering the softening behavior of quasi-brittle materials. Two different optimization strategies are presented: a fully nonlinear strategy and a simplified strategy. The fully nonlinear strategy relies on existing nonlinear damage models, which require iterative solution methods, for structural analysis and the computation of the corresponding sensitivities. The simplified strategy uses a simplified damage model, which computes a structure's damage distribution in only one step, greatly reducing computation time. The accuracy of the simplified damage model is controlled by occasional nonlinear simulations – without sensitivity analysis – to calibrate the results. Benchmark tests compare the simplified optimization strategy with the fully nonlinear optimization strategy. While the simplified damage model does not have the same accuracy as nonlinear damage models, results show similar optimized topologies and structural efficiency, with a significant improvement regarding computation time for the simplified optimization strategy.

KEYWORDS:
Topology design, damage, structures

1 | INTRODUCTION

For practical engineering applications, structures are typically designed to have a predefined load capacity at a minimal cost, ensuring that the structure does not fail under the design load. A possible strategy to automate this design process is topology optimization, which is the optimization of the material distribution within a design domain. In the original formulation of topology optimization, by Bendsøe and Kikuchi [1], a structure's mechanical performance is represented by its compliance, but while this concept allows for designing structures with a high stiffness, it is no direct measure for failure of a structure. Instead of elastic compliance, alternative concepts are required for the optimization of structures with a predefined load-bearing capacity.

One of the most intuitive strategies for designing or optimizing structures with a guaranteed load capacity is limiting the stress under a given load. If the level of stress in the entire structure is lower than the maximum allowable stress of the material, the structure will not fail. The topic of stress-constrained topology optimization has been widely investigated. Two possible

This article has been accepted for publication and undergone full peer review but has not been through the copyediting, typesetting, pagination and proofreading process which may lead to differences between this version and the Version of Record. Please cite this article as doi: 10.1002/nme.6891

strategies are constraint aggregation[2,3,4] and the augmented Lagrangian method[5,6,7].

The focus of this study lies on materials with highly nonlinear behavior, such as elastoplastic and strain-softening materials. Once a threshold for stress or strain is reached, the material loses part of its stiffness but may experience large deformations before actually failing. For such materials, failure cannot easily be expressed in terms of a maximal stress or strain. By constraining the stress to be lower than the yield stress, the optimized designs will be structurally safe but overly conservative, since the behavior beyond yielding or damage initiation is not considered.

Maute et al.[8] combined topology optimization with nonlinear elastoplastic material models, to better exploit the potential of elastoplastic materials. Russ and Waisman[9] suggested an elastoplastic topology optimization method to increase the failure resistance of structures with a fixed volume, by using local ductile failure constraints and linear buckling analysis. Strain-softening materials lose stiffness when strain reaches a certain threshold, and can be used to model damage processes such as micro-cracking in quasi-brittle materials. Several numerical models exist to simulate strain-softening damage, and they have been successfully utilized for topology optimization of damage-resistant structures, among others by Amir et al.[10,11], James and Waisman[12], Noël[13] and Da et al.[14].

Amir et al. developed a method for topology optimization of reinforced concrete structures[10] and reinforcement layout optimization for concrete structures with predefined geometries[11]. In both cases, a gradient-enhanced damage model is used to ensure damage-resistance of the optimized structure, by constraining the compliance of the damaged structure. James and Waisman[12] used a nonlocal damage model in topology optimization to increase damage-resistance, by simultaneously implementing a compliance constraint that considers damage, and a constraint on the maximal amount of damage in the structure. Noël[13] used the same nonlocal damage model as James and Waisman, but followed a level-set optimization approach. Da et al.[14] recently published work on the optimization of the fracture resistance of two-phase composites considering damage: relying on a phase-field damage model, structures consisting of two materials are optimized for maximal fracture resistance with a constant volume fraction of both materials. While above authors successfully combined topology optimization with nonlinear damage models for increased damage resistance, they did not solve the typical engineering problem, which is minimizing the weight or cost of a structure with a constraint on the load-bearing capacity. Formulating the exact constraint function is non-trivial, because the load capacity of a structure consisting of a quasi-brittle material is highly nonlinear with respect to the design variables.

This paper first presents two models for the simulation of the damaged behavior of structures. The first simulation model is a nonlinear strain-softening damage model, in the following simply referred to as the nonlinear damage model. It is based on the model used by Peerlings[15], and iteratively computes the damage distribution and damaged behaviour of structures. As a second simulation model, we propose a simplified model that computes a structure's damage distribution in a single step.

Based on these simulation models, we propose two novel optimization strategies for minimal weight optimization with an ultimate load constraint. The first strategy, called the fully nonlinear optimization strategy, relies completely on the nonlinear damage model. The second, simplified strategy uses the simplified one-step damage model for simulation and sensitivity analysis, combined with occasional simulations with the nonlinear damage model, to compensate for the reduced accuracy of the simplified damage model.

This article is structured as follows: Section 2 focuses on the simulation of damage, according to two approaches: (a) the nonlinear damage model presented by Peerlings[15], and (b) the novel one-step damage model developed for this study. Section 3 addresses the optimization of damage-resistant structures with minimal weight and a constraint on their load-bearing capacity. Both newly developed strategies are discussed: the fully nonlinear optimization strategy, and the faster simplified optimization strategy, which relies on the one-step damage model. Throughout Sections 2 and 3, a first case study is used for demonstration. In Section 4, two additional case studies are considered to test the general applicability and further compare the performance of both optimization strategies. The conclusions of this study are presented in Section 5.

2 | SIMULATION

Several approaches exist to simulate the propagation of damage, based on various models. Two simulation models will be discussed in detail: an existing nonlinear model and a simplified model that was developed for this study. Both simulation models rely on the general principles of strain-softening damage, which is explained first.

2.1 | Strain-softening damage

In the current study, the focus lies on quasi-brittle materials, experiencing strain-softening damage. For such materials, the damage distribution follows the strain distribution. At locations where a strain-based measure exceeds a certain threshold, damage is assumed and the stiffness at that location is reduced accordingly. The presented strain-softening damage model for quasi-brittle materials is based on the model used by Peerlings et al.[15].

Damage is represented by a scalar damage variable D, which is a function of the strain distribution in the structure. The stiffness E_d of the material is adapted depending on the intensity of damage:

$$E_\mathrm{d} = (1 - D)\, E_0 \tag{1}$$

where E_0 is the stiffness of the undamaged material. If the material is fully damaged, which corresponds to the damage variable D equal to one, the stiffness is reduced to zero.

As the first step for the computation of the damage variable D, an equivalent strain measure combines all strain components of the strain tensor $\boldsymbol{\epsilon}$ to a scalar equivalent strain ϵ_eq. The modified Von Mises criterion for strains, as developed by De Vree et al.[16], accounts for the difference in tensile and compressive strength of the material:

$$\epsilon_\mathrm{eq}(\boldsymbol{\epsilon}) = \frac{k-1}{2k(1-2\nu)} I_1 + \frac{1}{2k}\sqrt{\frac{(k-1)^2}{(1-2\nu)^2} I_1^2 + \frac{12k}{(1+\nu)^2} J_2} \tag{2}$$

where the parameter k expresses the ratio between compressive and tensile strength, and the parameter ν is the Poisson's ratio of the material. The first strain invariant I_1 is expressed as a function of the components ϵ_{ij} of the strain tensor $\boldsymbol{\epsilon}$:

$$I_1 = \mathrm{tr}(\boldsymbol{\epsilon}) = \epsilon_{11} + \epsilon_{22} + \epsilon_{33} \tag{3}$$

and the second deviatoric strain invariant J_2 is:

$$J_2 = \frac{1}{6}\left[(\epsilon_{11} - \epsilon_{22})^2 + (\epsilon_{22} - \epsilon_{33})^2 + (\epsilon_{33} - \epsilon_{11})^2\right] + \epsilon_{12}^2 + \epsilon_{23}^2 + \epsilon_{31}^2 \tag{4}$$

A strain history parameter κ is introduced, which represents the highest achieved value of the equivalent strain at a given time, to capture the irreversible character of damage:

$$\kappa = \max(\kappa_\mathrm{old}, \epsilon_\mathrm{eq}) \tag{5}$$

If the equivalent strain ϵ_eq increases, the history parameter κ will increase too, but if the equivalent strain ϵ_eq decreases, the history parameter κ will remain constant. This ensures that damage never decreases, even when the strains in the structure decrease. Because of the irreversibility of damage, the solution becomes path-dependent. To best approximate the correct

loading path, an external load or displacement should be imposed gradually, and not instantaneously.

Finally, the strain history parameter κ is translated to the damage variable D, by means of an exponential damage law proposed by Peerlings et al.[15]:

$$D = \begin{cases} D_A = 0 & \text{if} \quad \kappa \leq \kappa_0 \\ D_B = 1 - \frac{\kappa_0}{\kappa}\left(1 - \alpha + \alpha \exp(-\beta(\kappa - \kappa_0))\right) & \text{if} \quad \kappa > \kappa_0 \end{cases} \tag{6}$$

with material parameters α and β. As long as the equivalent strain is lower than the strain threshold κ_0, damage is equal to zero. When the strain threshold is exceeded, damage is described by D_B and increases asymptotically to one, which corresponds to a total loss of stiffness.

The discrete damage law is smoothed using an adaptation of a Kreisselmeier-Steinhauser (KS) envelope[17], which combines the functions D_A and D_B in one smooth function D_s approximating the maximum of both functions (see Figure 1), to ensure the differentiability of the damage parameter D. The original KS envelope, as used by e.g. Amir[10] and Noël[13], returns values greater than one for D_B equal to one, which leads to a negative stiffness of the material. In practice, this is often solved by limiting the value of the smooth damage D_s to a value slightly lower than one. As an alternative, we propose an adapted version of the KS envelope, which ensures that the smooth damage remains strictly lower than or equal to one:

$$D_s = \frac{\ln(1 + \exp(c_s D_B))}{\ln(1 + \exp(c_s))} \tag{7}$$

where parameter c_s determines the sharpness of the smooth approximation.

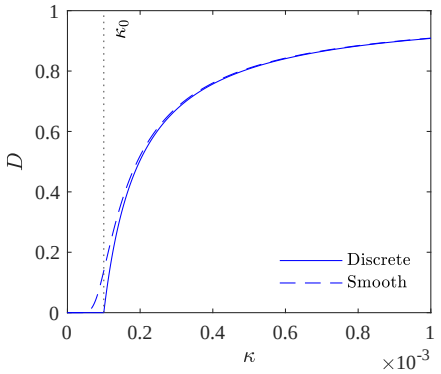

FIGURE 1 Discrete and smooth formulation of the exponential damage law. ($\alpha = 0.95$, $\beta = 100$, $c_s = 5$, $\kappa_0 = 1 \times 10^{-4}$)

2.2 | Finite element discretization

In this study, the finite element method is used for structural analysis. We consider only two-dimensional structures, represented by a regular grid of square finite elements. These are 4-node isoparametric elements with 2 degrees of freedom in each node, i.e. horizontal and vertical displacement.

2.2.1 | Nonlinear damage model

We consider the finite element discretization of the strain-softening damage model as implemented by Peerlings et al.[18] With the so-called gradient enhanced damage model, the mechanical behavior of a damaged structure is governed by two partial

differential equations. First, the static equilibrium of the structure is described by:

$$\boldsymbol{\nabla} \cdot \boldsymbol{\sigma} = \mathbf{0} \tag{8}$$

The second partial differential equation avoids the numerical issue of damage localization, as first shown by Bažant and Pijaudier-Cabot[19]. If no minimal length scale is imposed on the damage distribution, damage can remain concentrated in one or more finite elements, leading to mechanical behavior that is severely mesh-dependent and physically meaningless. To prevent localization, the original equivalent strains ϵ_{eq} are translated to the nonlocal equivalent strains $\bar{\epsilon}_{\text{eq}}$. The averaging equation imposes a length scale on the nonlocal equivalent strain distribution:

$$\bar{\epsilon}_{\text{eq}} - c\nabla^2 \bar{\epsilon}_{\text{eq}} = \epsilon_{\text{eq}} \tag{9}$$

where gradient parameter c, expressed as a surface area, ensures a minimal length scale or characteristic length l_{c} of the nonlocal equivalent strains $\bar{\epsilon}_{\text{eq}}$, and therefore also of the damage in the structure, eliminating localization issues:

$$c = 0.5\, l_{\text{c}}^2 \tag{10}$$

The state variables, which are the displacements $\mathbf{u}$ and nonlocal equivalent strains $\bar{\boldsymbol{\epsilon}}_{\text{eq}}$ can only be computed iteratively, because of the nonlinearity of the problem. The displacement vector is computed as follows:

$$\mathbf{u}_i = \mathbf{u}_{i-1} + \delta\mathbf{u}_i \tag{11}$$

where the subscript i refers to the iteration number, $\mathbf{u}_i$ is the displacement vector at iteration i, and $\delta\mathbf{u}_i$ is a correction term.

Similarly, the equivalent strain vector at iteration i is expressed as:

$$\bar{\boldsymbol{\epsilon}}_{\text{eq},i} = \bar{\boldsymbol{\epsilon}}_{\text{eq},i-1} + \delta\bar{\boldsymbol{\epsilon}}_{\text{eq},i} \tag{12}$$

with the correction term $\delta\bar{\boldsymbol{\epsilon}}_{\text{eq},i}$.

To compute the linearized change of the state variables, both partial differential equations are transformed to a discretized weak form, using partial integration and following the Galerkin approach. For a detailed explanation of this procedure, we refer to section 4 of the article by Peerlings et al.[18] The change of the state variables can be found by solving the following coupled system of equations:

$$\begin{bmatrix} \mathbf{K}_{i-1}^{uu} & \mathbf{K}_{i-1}^{u\epsilon} \\ \mathbf{K}_{i-1}^{\epsilon u} & \mathbf{K}^{\epsilon\epsilon} \end{bmatrix} \begin{bmatrix} \delta\mathbf{u}_i \\ \delta\bar{\boldsymbol{\epsilon}}_{\text{eq},i} \end{bmatrix} = \begin{bmatrix} \mathbf{f}_{\text{ext}}^{u} - \mathbf{f}_{\text{int},i-1}^{u} \\ \mathbf{f}_{i-1}^{\epsilon} - \mathbf{K}^{\epsilon\epsilon}\, \bar{\boldsymbol{\epsilon}}_{\text{eq},i-1} \end{bmatrix} \tag{13}$$

where the right-hand term contains the residuals of the discretized weak forms of the governing differential equations (8) and (9). The vectors $\mathbf{f}_{\text{ext}}^{u}$ and $\mathbf{f}_{\text{int},i-1}^{u}$ contain the nodal values of the external and internal forces, respectively. The superscript u is added to make a clear distinction with the fictitious load vector $\mathbf{f}_{i-1}^{\epsilon}$, which depends on the local equivalent strain distribution:

$$\mathbf{f}_{i-1}^{\epsilon} = \int_{\Omega} \tilde{\mathbf{N}}^{\text{T}} \epsilon_{\text{eq},i-1}\, \text{d}\Omega \tag{14}$$

The matrix on the left-hand side of equation (13) is the tangential matrix, which describes the linearized relation between the

state variables and the residuals. The tangential matrix consists of the following parts:

$$\mathbf{K}^{uu}_{i-1} = \int_{\Omega} \mathbf{B}^{\mathrm{T}}(1-D)\mathbf{C}\mathbf{B}\, d\Omega \tag{15}$$

$$\mathbf{K}^{u\epsilon}_{i-1} = -\int_{\Omega} \mathbf{B}^{\mathrm{T}}\mathbf{C}\boldsymbol{\epsilon}_{i-1} q_{i-1}\tilde{\mathbf{N}}\, \mathrm{d}\Omega \tag{16}$$

$$\mathbf{K}^{\epsilon u}_{i-1} = -\int_{\Omega} \tilde{\mathbf{N}}^{\mathrm{T}} \left(\frac{\partial \epsilon_{\mathrm{eq}}}{\partial \boldsymbol{\epsilon}}\right)^{\mathrm{T}} \mathbf{B}\, d\Omega \tag{17}$$

$$\mathbf{K}^{\epsilon\epsilon} = \int_{\Omega} \left(\tilde{\mathbf{N}}^{\mathrm{T}}\tilde{\mathbf{N}} + \tilde{\mathbf{B}}^{\mathrm{T}} c \tilde{\mathbf{B}}\right) \mathrm{d}\Omega \tag{18}$$

where the parameter q in equation (16) denotes the derivative of damage with respect to the strain history parameter κ. The scalar q is therefore only non-zero if damage is increasing:

$$q = \begin{cases} \frac{\partial D}{\partial \kappa} & \text{if} \quad \bar{\epsilon}_{\mathrm{eq}} > \kappa_{\mathrm{old}} \\ 0 & \text{if} \quad \bar{\epsilon}_{\mathrm{eq}} \leq \kappa_{\mathrm{old}} \end{cases} \tag{19}$$

If the external load $\mathbf{f}^{u}_{\mathrm{ext}}$ on the structure is known, equation (13) can be solved with a standard Newton-Raphson solver. However, the optimization strategies in this study rely on a displacement-based loading scenario. The required displacement of a point in the structure is imposed, and the spatial distribution of the load is defined by the user. We use the displacement-based Newton-Raphson scheme by Batoz and Dhatt[20] to indirectly search the corresponding load multiplier to achieve the imposed displacement of the structure. The problem is solved iteratively until the norm n_{r} of the residuals converges to a value below the user-defined threshold for convergence, which is chosen as 10^{-3} for this study:

$$n_{\mathrm{r}} = \frac{\left\| \begin{bmatrix} \mathbf{f}^{u}_{\mathrm{ext}} - \mathbf{f}^{u}_{\mathrm{int},i-1} \\ \mathbf{f}^{\epsilon}_{i-1} - \mathbf{K}^{\epsilon\epsilon}\,\bar{\boldsymbol{\epsilon}}_{\mathrm{eq},i-1} \end{bmatrix} \right\|}{\left\| \begin{bmatrix} \mathbf{f}^{u}_{\mathrm{ext}} \\ \mathbf{f}^{\epsilon} \end{bmatrix} \right\|} \tag{20}$$

Because the formulation of the tangent stiffness matrix is consistent, the convergence of the Newton-Raphson solver is expected to be quadratic. However, in practice, the solution does not always converge and even diverges in certain cases, with the norm n_{r} of the residuals increasing after each iteration. A possible solution for this problem is using a quasi-Newton solver, which replaces the exact tangent stiffness matrix by an approximation, increasing the stability of the solution, but at a lower rate of convergence.

In the presented cases, the problem of divergence was mainly caused by the derivative q of damage, which can assume values that are multiple orders of magnitude higher than the other terms in the tangent stiffness matrix. If the solution diverges, which is assumed when the norm n_{r} exceeds a certain threshold, chosen as 10^{3} for this study, we reduce parameter q in equation (16) by a factor 10. The system of equations is solved again with the modified tangent stiffness matrix. If the norm n_{r} exceeds the threshold again, the parameter q is further reduced by a factor 10. For the following computations, the value of q is reset to the original, to regain quadratic convergence.

The stiffness of the finite elements is reduced based on damage in each of the four Gauss points per element.

2.2.2 | One-step damage model

To reduce the computation time required for the nonlinear damage model, a simpler model is developed that captures only first-order effects of damage. Instead of using an iterative, path-dependent strategy, the damage distribution is now calculated in a single step, without additional iterations, based on the elastic strain distribution of the structure. Note that the name "one-step damage model" was chosen because the damage distribution is computed in one step. One might also argue that the model requires two steps, a first elastic step to compute damage, and a second step to compute the increased displacements considering damage.

The structure is loaded with the one-step load vector $\mathbf{f}_{\text{os}}$, and its displacements $\mathbf{u}$ are obtained from the following equation:

$$\mathbf{f}_{\text{os}} = \mathbf{K}_0 \, \mathbf{u} \tag{21}$$

where $\mathbf{K}_0$ is the elastic stiffness matrix, computed with the initial undamaged material.

The elastic strains in the structure are computed from the displacement vector $\mathbf{u}$. Using equation (2), the elastic strain components ϵ_{ij} are translated to equivalent strains ϵ_{eq}. The damage history parameter κ is identical to the equivalent strain ϵ_{eq} because damage is computed in a single step. The damage variable D is found with the smooth version of the exponential damage law (7). The stiffness of each element is reduced according to the amount of damage, as described by equation (1).

The stiffness matrix $\mathbf{K}_{\text{d}}$ is constructed based on the reduced stiffness per element, and links the one-step load vector $\mathbf{f}_{\text{os}}$ with the displacement vector $\mathbf{u}_{\text{d}}$, considering one-step damage:

$$\mathbf{f}_{\text{os}} = \mathbf{K}_{\text{d}} \, \mathbf{u}_{\text{d}} \tag{22}$$

For the one-step damage model, the magnitude of the applied load $\mathbf{f}_{\text{os}}$ must be chosen. The displacement vector $\mathbf{u}_{\text{d}}$ is identical to the elastic displacement vector $\mathbf{u}$ for loads that are infinitesimally small. Higher loads lead to a larger amount of damage in the structure, leading to a more pronounced nonlinear softening effect. The choice of the one-step load has a large impact on the damage-resistance or material efficiency of optimized structures. In general, the one-step load should be chosen so that the approximated damage is somehow representative for the real amount of damage. An automated strategy for selecting an adequate load will be discussed at the end of Section 3.2.2.

For simplicity, damage is only considered at the center of each finite element, as opposed to the nonlinear damage model, where damage is considered in four Gauss points per element. While the nonlinear damage model is sensitive to localization issues, no specific measures to prevent localization are required for the one-step damage model, since the distribution of damage is purely based on the elastic strain distribution of the structure.

2.3 | Load-displacement curve

In the following, the load vector $\mathbf{f}$ is defined as the the product of a scalar load multiplier f representing the physical magnitude of the total load, and a dimensionless vector $\mathbf{p}$ representing the spatial distribution of the load:

$$\mathbf{f} = f \, \mathbf{p} \tag{23}$$

In this study, all loads are distributed over multiple nodes, to avoid stress or damage singularities.

We define the scalar displacement u to represent the displacement at the so-called displacement-control degree of freedom (DOF) of the structure:

$$u = \mathbf{l}^{\mathrm{T}}\mathbf{u} \tag{24}$$

where selection vector $\mathbf{l}$ selects the correct component of the displacement vector $\mathbf{u}$.

In order to compose a structure's load-displacement curve $f(u)$, following a displacement-controlled loading sequence, the desired displacement u at the displacement-control DOF is increased in steps Δu_{ld} and the required load multiplier f to achieve that displacement is plotted on the vertical axis (see Figure 2). The maximal load in the load-displacement curve is the load resistance f_{r} of the structure:

$$f_{\mathrm{r}} = \max_{u}(f(u)) = f(u_{\mathrm{r}}) \tag{25}$$

where displacement u_{r} is the displacement of the structure at the point of failure, which occurs when load f_{r} is applied. A structure's load resistance is equal to its ultimate load-bearing capacity, since an attempt to apply a higher load would lead to unbounded displacements. When designing a structure, the load resistance should always be greater than or equal to the design load. In practice, safety margins are considered to guarantee structural integrity, even under extreme circumstances. For simplicity, we don't consider such safety margins in this study, but a similar effect can be obtained by artificially increasing the design load or decreasing the mechanical performance of the material.

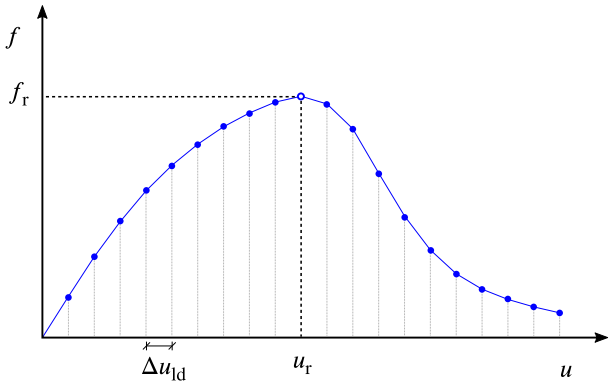

FIGURE 2 Load-displacement curve for displacement-controlled loading sequence, with load resistance f_{r} and corresponding displacement u_{r}.

2.4 | Example

To compare the two damage models, we consider an L-shaped bracket, which is a frequently used example in stress-constrained topology optimization. The bracket measures 6 by 6 meters, and is modeled with 120 by 120 finite elements (see Figure 3). The bracket is clamped at the top and loaded vertically at the right-hand side. The detail in Figure 3 shows the load distribution vector $\mathbf{p}$, which divides the vertical load over 11 nodes in the center of the right-hand edge, with the first and last node carrying half the load of the other nodes. Table 1 contains a summary of all material characteristics. The displacement-control DOF is the vertical displacement of the central node on the right-hand side, shown as a green dot in Figure 3. The thickness of the structure is 1 m and plane stress is assumed.

TABLE 1 Material parameters for the L-bracket example.

α	β	k	c_s	l_c [m]	E [MPa]	ν	κ_0
0.95	100	5	5	0.15	30×10^3	0.2	1×10^{-4}

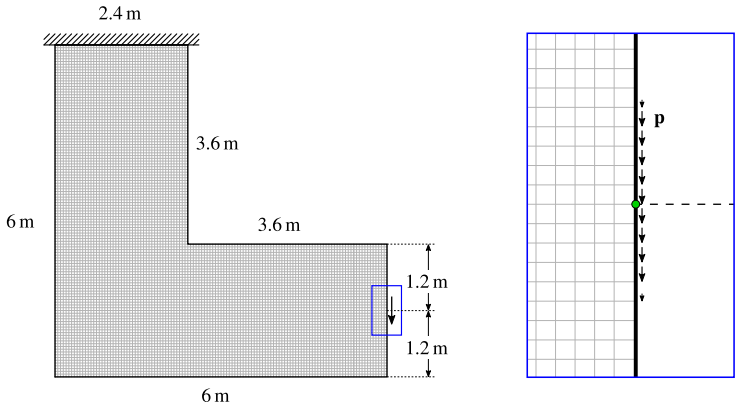

FIGURE 3 Dimensions and boundary conditions of the L-bracket. The right-hand side shows the load distribution and the displacement-control DOF.

Using the nonlinear damage model, the structure's load-displacement curve is constructed for a displacement of 0 to 20 mm in 40 displacement steps Δu_{ld} of 0.5 mm (see Figure 4). The load resistance f_r of the solid structure is 697.0 kN, at a displacement u_r of 8 mm. Figure 5a shows the damage distribution for a displacement of 3 mm. As expected, damage emerges at the re-entrant corner of the bracket, where a stress concentration occurs.

With the one-step damage model, an arbitrarily selected load f_{os} of 1000 kN leads to the damage distribution as shown in Figure 5b. Under this load, the elastic displacement u is 3.94 mm and the displacement u_d, considering one-step damage, is 5.43 mm.

Figure 5 compares the damage distribution computed with both damage models. In both cases, damage emerges mainly in regions of the structure that experience tension, since the material is modeled to be five times stronger in compression than

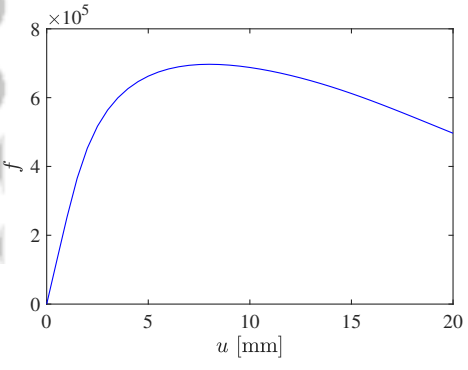

FIGURE 4 Load-displacement curve of the solid L-bracket, computed with the nonlinear damage model.

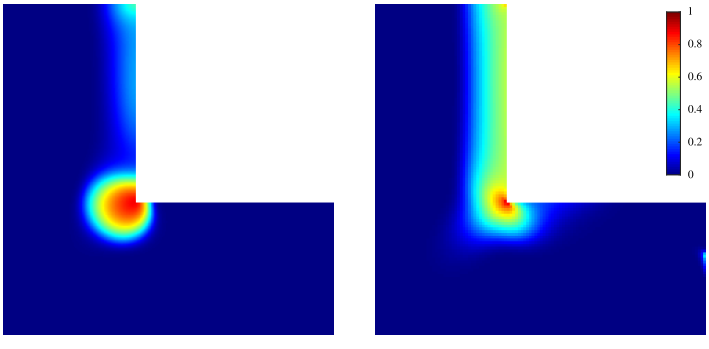

(a) Nonlinear damage model **(b)** One-step damage model

FIGURE 5 Damage distribution in a solid L-bracket, computed with both damage models.

in tension, as defined in equation (2) with k equal to 5. With the nonlinear model, damage is concentrated mainly at the re-entrant corner and only to a lesser extent along the vertical leg of the bracket. The simplified damage model leads to a more uniform distribution of damage around the re-entrant corner, and along the vertical leg. This difference can be explained by the accumulation of damage with the nonlinear model. Damage emerges initially at the re-entrant corner, leading to a local reduction of stiffness in that location. Due to the reduction of stiffness, strains at the re-entrant corner increase, leading to increasingly large amounts of damage at each iteration. The one-step damage model does not experience such accumulation of damage, since damage is only computed once. Nevertheless, as it will be demonstrated later, the one-step damage model adequately captures damage during the optimization process.

3 | OPTIMIZATION

For this study, we rely on density-based topology optimization to find structures with a predefined load capacity and a minimal weight. We discuss the design parameterization and formulation of the optimization first.Section 3.3 extends the proposed methodology with the robust projection method by Wang et al.[21], to increase the discreteness of the solution and add a length scale to the optimized design.

3.1 | Design parameterization

All structures are represented by a two-dimensional grid of square finite elements with varying densities $\tilde{\rho}_e$. These element densities, which are dimensionless values between 0 (void) and 1 (solid), describe the presence or absence of material for each element. If the element densities $\tilde{\boldsymbol{\rho}}$ would be used as design variables in the optimization problem, the solution would be mesh-dependent[22] and checkerboard patterns could emerge[23]. Therefore, a distinction is made between the design variables $\boldsymbol{\rho}$ and the element densities $\tilde{\boldsymbol{\rho}}$, and the relation between both is expressed as a spatial averaging operation, referred to as a density filter:

$$\tilde{\rho}_e = \frac{\sum_{i=1}^{N} w_{ei} v_i \rho_i}{\sum_{i=1}^{N} w_{ei} v_i} \tag{26}$$

where N is the total number of elements, v_i is the volume of an element i, and w_{ei} is a weight factor, depending on the center-to-center distance r_{ei} between elements e and i, and the filter radius r:

$$w_{ei} = \max(0, r - r_{ei}) \tag{27}$$

As an alternative, one could also use a PDE filter[24], which is based on a partial differential equation similar to (9).

The stiffness of each element depends on the element density $\tilde{\rho}_e$ and the amount of damage D_e:

$$E_{\mathrm{d}} = E_{\min} + (1 - D_e)\, \tilde{\rho}_e^{p}\, (E_0 - E_{\min}) \tag{28}$$

where penalization parameter p penalizes intermediate densities, based on the solid isotropic material with penalization (SIMP) method[25]. The penalization parameter p is equal to 3 for all examples in this article. Young's modulus E_0 represents the stiffness of the solid, undamaged material. A minimal stiffness $E_{\min}$ which is 10^9 times lower than the stiffness E_0 avoids singularity of the finite element equations for elements with a density equal to zero or damage equal to one. A filter radius r of 0.25 m is used for the L-bracket.

3.2 | Formulation of the optimization problem

The optimization problem is ideally formulated as follows: "Find the structure with the least amount of material that has an ultimate load capacity higher than or equal to a user-defined design load." This translates to a minimization of the material

volume, with a constraint on the load resistance f_r, which should be greater than or equal to the design load f_d:

$$\begin{aligned} \min_{\rho}: \quad & V = \frac{\sum_e v_e \tilde{\rho}_e}{\sum_e v_e} \\ \text{s.t.}: \quad & f_r \geq f_d \\ & 0 \leq \rho_e \leq 1 \end{aligned} \tag{29}$$

where V is the volume fraction of the design, which represents the material volume as a fraction of the total volume of the design domain.

Because the load resistance f_r of a structure is not differentiable with respect to the design variables $\boldsymbol{\rho}$, the optimization problem must be reformulated with an alternative, differentiable constraint function. Two adaptive optimization strategies are proposed to indirectly solve the original optimization problem (29): a fully nonlinear optimization strategy and a simplified strategy based on the one-step damage model.

3.2.1 | Fully nonlinear optimization strategy

The first strategy relies completely on the nonlinear damage model, as described in Section 2.2.1. While it is not possible to differentiate the load resistance f_r with respect to the design variables, it is possible to differentiate the load f for a predefined imposed displacement u_i. The original optimization problem is reformulated as:

$$\begin{aligned} \min_{\rho}: \quad & V = \frac{\sum_e v_e \tilde{\rho}_e}{\sum_e v_e} \\ \text{s.t.}: \quad & f(u_i) \geq f_d \\ & 0 \leq \rho_e \leq 1 \end{aligned} \tag{30}$$

Note that this formulation is only equivalent to the original optimization problem (29) if the imposed displacement u_i is equal to the displacement u_r of the optimized structure, since the required load to achieve a displacement u_r is equal to the load resistance f_r:

$$f(u_r) = f_r \tag{31}$$

An adaptive optimization strategy has been developed, which consists of a sequence of optimization loops and parameter updates. After convergence of each loop of the optimization problem (30), the value of the imposed displacement u_i is adapted to match the displacement u_r of the current design (see Figure 6). The optimization loop is performed again with the updated

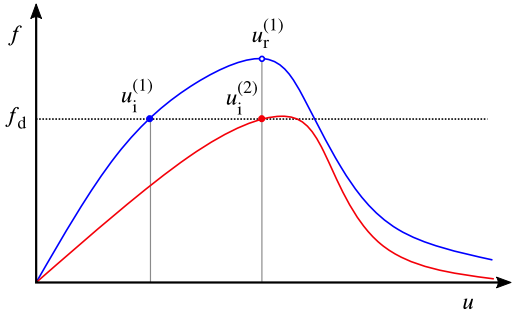

FIGURE 6 Graphical representation of the parameter update for the fully nonlinear optimization strategy. The imposed displacement u_i is adapted to match the displacement u_r of the previous iteration.

imposed displacement and the process is repeated.

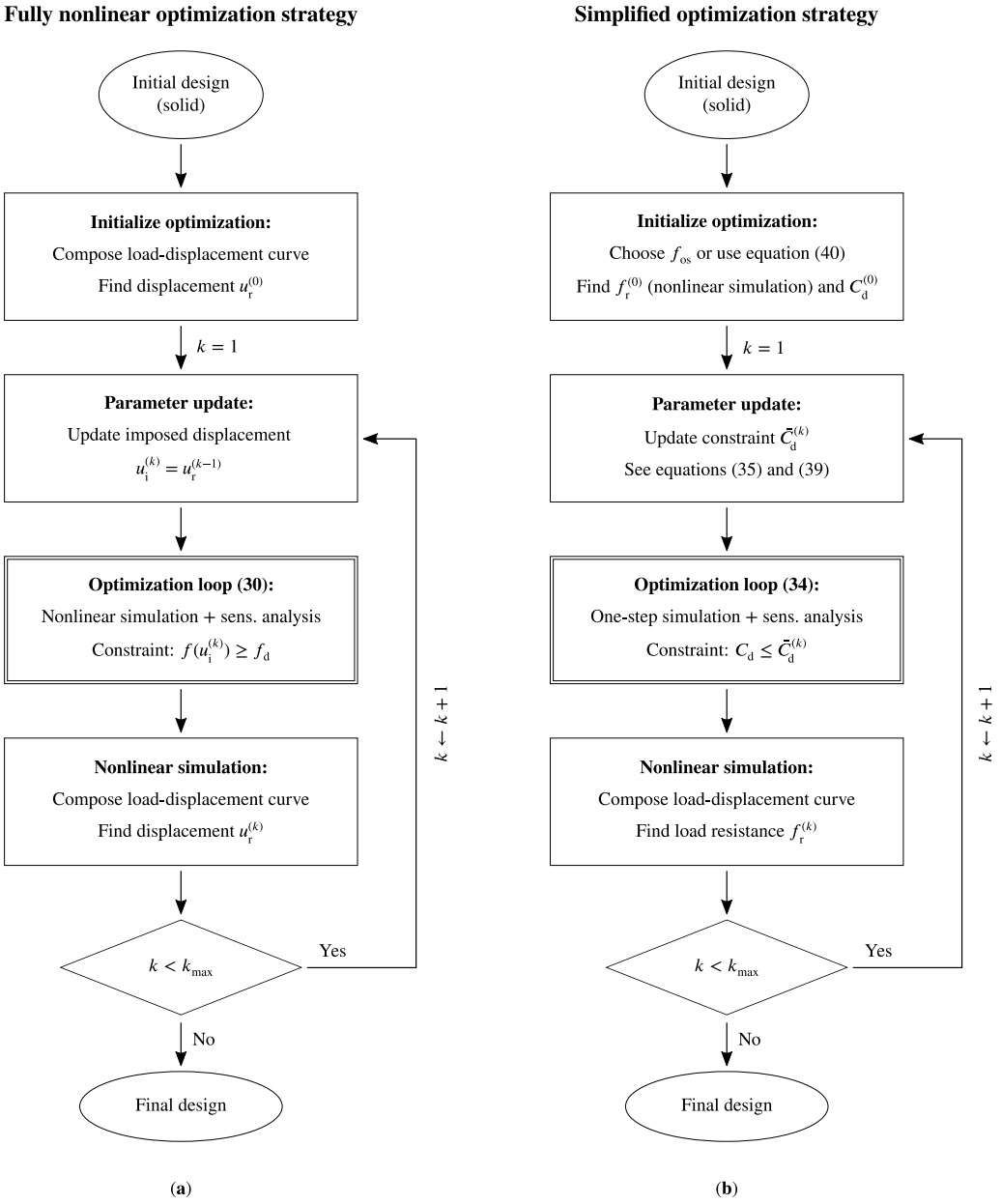

FIGURE 7 Flow charts describing fully nonlinear (a) and simplified (b) optimization strategy.

For the practical implementation (see Figure 7), the optimization algorithm starts from a user-defined initial design. The initial design is chosen to be a solid structure, with all element densities $\tilde{\rho}_e$ set to one. By starting from a solid structure, the maximal achievable load resistance can be estimated. If the load resistance of the solid structure is lower than the design load, the chance of finding a feasible design is small, and the optimization problem, boundary conditions or design load may have to be adapted. Based on the solid structure, a number of parameters for the optimization strategy is initialized. The size of the displacement steps Δu_{ld} to compute the load-displacement curve must be chosen before performing a nonlinear simulation. As a general rule, smaller displacement steps lead to a more accurate characterization of the load-displacement curve, at the cost

of increased computation time. If the displacement step is too large, for example larger than the displacement u_r, the load resistance of the structure will be severely underestimated. A displacement step Δu_{ld} of 0.5 mm is chosen for the L-bracket example.

The load-displacement curve of the solid structure is computed, to find the displacement u_r. As soon as a local maximum is found, the current load f is assumed to be equal to the load resistance f_r, and the simulation is terminated. For the L-bracket, the displacement u_r is reached after 16 displacement steps, since the load f decreases at the following displacement step.

After initialization, the imposed displacement u_i is updated to match the displacement u_r. Using the method of moving asymptotes (MMA) developed by Svanberg[26], the weight of the structure is minimized, while ensuring the load at the imposed displacement $f(u_i)$ remains larger than or equal to the design load f_d. While this ensures that the structure can support the design load, a large difference between the imposed displacement u_i and displacement u_r suggests that the structure is overly conservative, because the actual load resistance f_r is likely to be higher than the design load. The sensitivity analysis for this optimization problem is found in the literature, such as Amir[10].

To increase the accuracy of the simulation, the imposed displacement u_i is not applied instantaneously, but in a number of steps $\Delta u_i^{(k)}$. To capture most of the path-dependence at a reasonable computational cost, we choose to apply the total imposed displacement in 4 steps:

$$\Delta u_i^{(k)} = \frac{1}{4} u_i^{(k)} \tag{32}$$

Note that these imposed displacement steps $\Delta u_i^{(k)}$ are different from the displacement steps Δu_{ld} for computing the structure's load-displacement curve, where we aim for a higher resolution. The size of the imposed displacement steps $\Delta u_i^{(k)}$ changes at every parameter update, whereas the size of the displacement steps Δu_{ld} remains fixed throughout the optimization.

After a predefined number of iterations, the optimization loop is terminated. The load-displacement curve is computed for the newly optimized design, using displacement steps Δu_{ld}, to find the displacement u_r. If the maximum number of parameter updates is not reached yet, the update counter k is increased and the imposed displacement u_i is updated to match the displacement u_r. This process is repeated until a maximum number of parameter updates is reached. For this study, each optimization loop consists of 25 iterations, and the imposed displacement is adapted 12 times, leading to a total of 300 design iterations.

As a first example, the L-bracket is optimized to support a design load of 500 kN. The material parameters and optimization parameters are shown in Tables 1 and 2, respectively. The passive elements, which are highlighted in the detail of Figure 8, have a fixed density of 1 throughout the optimization. These passive elements are necessary to obtain a stable convergence of the optimization for the fully nonlinear optimization strategy, by avoiding damage near the applied load. The resulting topology is shown in Figure 9, and the load-displacement curve of the optimized design is shown in Figure 10. The final design has an optimized volume fraction of 0.527, and the optimization process lasted 3 hours and 26 minutes. The optimization was performed with MATLAB version R2020b, on a Dell XPS 13 9370 laptop with 16 GB of RAM and an Intel Core i7-8550U processor, with the Windows 10 Pro operating system.

TABLE 2 Optimization parameters for the L-bracket example.

E_0 [MPa]	E_{min} [MPa]	r [m]
30×10^3	30×10^{-6}	0.25

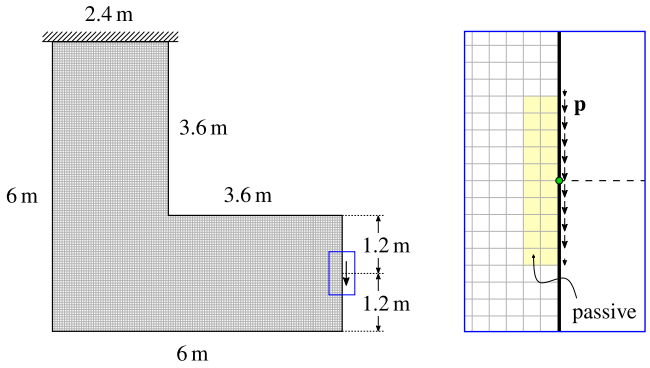

FIGURE 8 Dimensions and boundary conditions of the L-bracket. The passive elements are highlighted in yellow.

FIGURE 9 Optimized L-bracket design, using the fully nonlinear optimization strategy.

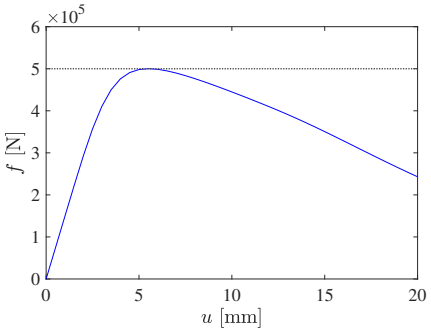

FIGURE 10 Load-displacement curve of the fully nonlinearly optimized L-bracket. The dotted line represents the design load.

Table 3 shows the detailed computation time. A distinction is made between the computation time of the so-called optimization loop, and the nonlinear simulation of the load-displacement curves. For the 'optimization loop' category, which is also indicated by a double box in Figure 7, we consider the computation time of the finite element analysis, the corresponding sensitivity analysis, and the MMA optimization algorithm[26]. The 'load-displacement simulation' category shows the time for computing the load-displacement curve after every optimization loop of 25 iterations, as well as the time required for initializing the load-displacement computation process at the beginning of the optimization.

TABLE 3 Comparison of the fully nonlinear and simplified optimization strategy, tested on the L-bracket example.

	Fully nonlinear	**Simplified**	
		$f_{os} = 1000\,\text{kN}$	Elastic
Volume fraction	0.527	0.594	0.715
Computation time (hh:mm:ss)			
– Optimization loop	03:09:40	00:04:59	00:03:10
– Load-displacement simulation	00:16:36	00:13:59	00:13:40
– Total	03:26:16	00:18:59	00:16:51

3.2.2 | Simplified optimization strategy

To reduce the computation time, we propose a faster method which uses the one-step damage model in combination with occasional nonlinear simulations. Similar to the fully nonlinear optimization strategy, the simplified optimization strategy uses a sequence of optimization loops and parameter updates. Instead of using the nonlinear damage model for the optimization loop, the simplified optimization strategy uses the one-step damage model. We introduce the one-step compliance C_d, based on the one-step load vector $\mathbf{f}_\mathrm{os}$ and the displacement vector $\mathbf{u}_\mathrm{d}$, as defined in equation (22):

$$C_\mathrm{d} = \mathbf{f}_\mathrm{os}^\mathrm{T}\,\mathbf{u}_\mathrm{d} \tag{33}$$

The optimization loop minimizes the material volume, subject to a constraint on the one-step compliance C_d:

$$\begin{aligned} \min_{\boldsymbol{\rho}}: \quad & V = \frac{\sum_e v_e \tilde{\rho}_e}{\sum_e v_e} \\ \text{s.t.}: \quad & C_\mathrm{d} \leq \bar{C}_\mathrm{d} \\ & 0 \leq \rho_e \leq 1 \end{aligned} \tag{34}$$

Although the one-step compliance C_d is not directly related to the load resistance f_r of a structure, tests show that designs with a lower compliance generally have a greater load resistance. Using a heuristic update method, the one-step compliance constraint $\bar{C}_\mathrm{d}$ is adapted after each optimization loop, indirectly leading to a design that satisfies the original constraint on the load resistance f_r. Contrary to the fully nonlinear optimization strategy, the reformulated optimization problem (34) is never equivalent to the original formulation (29). Nevertheless, tests show that similar optimized results are obtained at a much lower computational cost.

In a practical implementation (see Figure 7), the procedure starts from a solid design. Before starting the optimization, an adequate choice of the one-step load f_os must be made, since it determines the quality of the optimized results. If the one-step load is too small, the compliance C_d is almost equal to the elastic compliance C, and the optimized result will be similar to an elastically optimized result, with little damage resistance. For increasing values of the one-step load, the behavior of the structure is increasingly nonlinear. However, for excessively high values of the one-step load, convergence becomes problematic and the optimized designs are observed to be sub-optimal. Same as the simulation in Section 2.4, a one-step load of 1000 kN is chosen. At the end of this section, we describe a heuristic procedure for selecting an adequate one-step load.

During the initialization, the damaged compliance $C_\mathrm{d}^{(0)}$ of the solid structure is computed under the load f_os. The load-displacement curve is constructed and the peak load $f_\mathrm{r}^{(0)}$ is computed using the nonlinear damage model. The displacement step size Δu_ld, for computing the load-displacement curve, is chosen as 0.5 mm for the L-bracket example.

After initialization, a heuristic update method adapts the damaged compliance constraint without the need for a sensitivity analysis. In general, if the load resistance exceeds the design load, the design is overly conservative and the compliance constraint can be relaxed. Otherwise, the design does not meet the required load capacity and the compliance constraint is tightened. For the first parameter update, the value of the constraint $\bar{C}_\mathrm{d}^{(1)}$ is based on the compliance $C_\mathrm{d}^{(0)}$ of the initial solid design.

$$\bar{C}_\mathrm{d}^{(1)} = 1.5\, C_\mathrm{d}^{(0)} \tag{35}$$

For the following parameter updates, the new value of the compliance constraint is based on an extrapolation of the previous iterations. The compliance constraint and load resistance of the previous iterations are represented in two-dimensional space,

and following a least-squares approach, a curve is fitted through these data points (see Figure 11). The new value of the compliance constraint $\bar{C}_{\mathrm{d}}^{(k)}$ is found at the intersection of the fitted curve with the design load f_{d}.

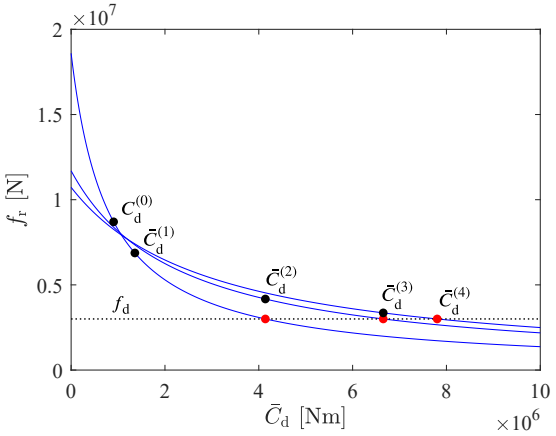

FIGURE 11 Reciprocal curve fitted through 2, 3 and 4 data points. The red dots show the intersection of the curve with the design load f_{d}, represented by a dotted line.

For the theoretical example of a one-dimensional bar which is loaded uniaxially, the elastic compliance C is inversely proportional to the load resistance f_{r}. Since this relation no longer exactly holds for more complex cases, we use a more general reciprocal function to approximate the relation between one-step compliance and load resistance, similar to the convex approximations used in MMA[26]:

$$f_{\mathrm{r}} = \frac{A}{\bar{C}_{\mathrm{d}} - B} \tag{36}$$

We impose that the curve intersects with the data point of the most recent parameter update:

$$f_{\mathrm{r}}^{(k-1)} = \frac{A}{\bar{C}_{\mathrm{d}}^{(k-1)} - B} \tag{37}$$

This ensures that the updated compliance constraint follows the general rule that a more relaxed constraint leads to a lower load resistance. Parameter B can be eliminated based on equation (37), leading to a reciprocal curve which is only dependent on parameter A:

$$f_{\mathrm{r}}^{(k)} = \frac{A}{\bar{C}_{\mathrm{d}}^{(k)} - \bar{C}_{\mathrm{d}}^{(k-1)} + \dfrac{A}{f_{\mathrm{r}}^{(k-1)}}} \tag{38}$$

Parameter A is optimized so that the curve (38) fits best between all data points, as formulated by a least-squares problem. The updated compliance constraint can be found at the intersection of the fitted curve with the design load f_{d}:

$$\bar{C}_{\mathrm{d}}^{(k)} = \bar{C}_{\mathrm{d}}^{(k-1)} + \frac{A}{f_{\mathrm{d}}} - \frac{A}{f_{\mathrm{r}}^{(k-1)}} \tag{39}$$

After updating the compliance constraint, the optimization loop is performed again with the new compliance constraint, using MMA[26] as the optimizer. The sensitivity analysis of the one-step compliance C_d with respect to the element densities $\tilde{\boldsymbol{\rho}}$ is elaborated in the appendix.

After a predefined number of iterations of the optimization loop, the load-displacement curve of the design is computed again. The update counter k is increased by one, the constraint $\bar{C}_{\mathrm{d}}^{(k)}$ is updated, and the process is repeated until a maximal amount of parameter updates is reached. We choose the same number of iterations as for the fully nonlinear optimization strategy, to allow for a fair comparison of the results. Therefore, each optimization loop consists of 25 iterations, and the imposed displacement is adapted 12 times.

The L-bracket is optimized again for a design load of 500 kN, using the simplified optimization strategy with an arbitrarily chosen one-step load f_{os} of 1000 kN. Figure 12 shows the resulting topology of the optimized design, and Table 3 shows the optimized volume fraction and computation time. The load-displacement curve in Figure 13 demonstrates that the load resistance is almost identical to the design load, shown as a dotted line. The optimization process lasted 19 minutes, and the optimized design has a volume fraction of 0.594, which is 13% higher than the volume fraction of the fully nonlinearly optimized design. Regarding the total computation time, the simplified optimization strategy is approximately 11 times faster than the fully nonlinear strategy. Table 3 shows that the computation time of the nonlinear simulation is very similar for both optimization strategies, since they both rely on the same nonlinear simulation model for composing the load-displacement curve of the structure. The reduction of computation time is almost completely due to the speed-up of the optimization loop. The simplified optimization strategy is 38 times faster during the optimization loop, because it uses the one-step damage model instead of the nonlinear damage model.

FIGURE 12 Optimized L-bracket design, using the simplified optimization strategy, for a one-step load f_{os} of 1000 kN.

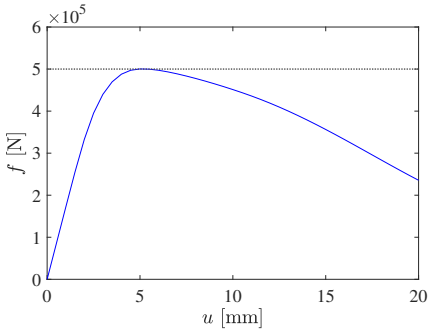

FIGURE 13 Load-displacement curve of the L-bracket, optimized with the simplified optimization strategy. The dotted line represents the design load.

Simplified optimization strategy with elastic compliance

To assess the impact of the one-step damage model, compared to a simple elastic model, the L-bracket structure is optimized again following the simplified optimization strategy, but with the elastic compliance C instead of the one-step compliance C_{d}. The optimized topology can be seen in Figure 14, and Figure 15 shows the corresponding load-displacement curve. Table 3 compares the volume fraction and computation time for the different optimization strategies. When compared with the fully nonlinear optimization strategy, the simplified elastic optimization strategy is about twelve times faster, but leads to a design which requires 36% more material. By using the elastic compliance instead of the one-step compliance C_{d} for the simplified optimization strategy, the computation time is further decreased by 11%, but the material volume increases with 20%.

Using the simplified elastic optimization strategy leads to minimal time savings, compared to the simplified optimization strategy with one-step damage. However, the material volume of the optimized design is significantly higher, because the elastic compliance does not reflect any difference in material behavior in tension and compression. Therefore, the simplified elastic optimization strategy will only be used as a reference in the following examples, to demonstrate the advantage of the nonlinear

FIGURE 14 Optimized L-bracket design, using the simplified elastic optimization strategy, with the elastic compliance C instead of the one-step compliance C_d.

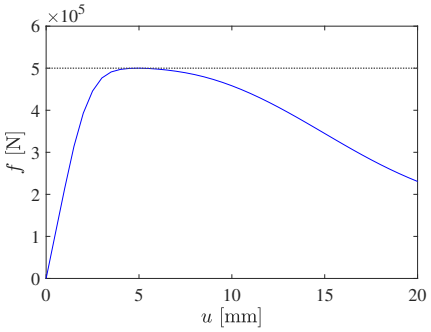

FIGURE 15 Load-displacement curve of the elastically optimized L-bracket. The dotted line represents the design load f_d.

damage model and the one-step damage model compared to a purely elastic material model for the optimization of damage-resistant structures.

Selecting the one-step load

We propose a heuristic method for finding an adequate value for the one-step load f_{os}, to increase the material efficiency of designs optimized with the simplified optimization strategy using the one-step damage model. The dimensionless damage percentile P_d is introduced, which describes the percentage of elements of the initial solid structure where the equivalent strain ϵ_{eq} exceeds the threshold for damage κ_0. During the initialization of the optimization, the solid structure is loaded with a unit load f_0, and the equivalent strains are computed for all elements and sorted in descending order. The equivalent strain corresponding to the percentile P_d is selected. Based on this selected equivalent strain $\epsilon_{eq}(P_d)$, the one-step load f_{os} is found:

$$f_{os} = \frac{\kappa_0}{\epsilon_{eq}(P_d)} f_0 \tag{40}$$

Under this one-step load f_{os}, the equivalent strain corresponding to P_d becomes equal to the damage threshold κ_0. Therefore, a percentage P_d of the equivalent strains in the solid structure is equal to or higher than the damage threshold.

To select an adequate value for the damage percentile P_d, the L-bracket problem has been optimized with the simplified strategy, for a range of values of the damage percentile. The solid blue line in Figure 16 shows the influence of the damage percentile on the volume fraction of the L-bracket, optimized for a design load of 300 and 500 kN, respectively. The results clearly show that values of the damage percentile close to zero or one lead to sub-optimal designs. For low values, the optimized volume fraction is similar to that of a design optimized with the elastic compliance C (blue dashed line in Figure 16). For a design load of 300 kN, values of the damage percentile P_d between 0.15 and 0.95 lead to material efficiencies similar to the design optimized with the fully nonlinear optimization strategy (red dash-dot line in Figure 16). For a design load of 500 kN, the volume fraction approaches that of the fully nonlinear optimized design for increasing values of the damage percentile, except when the percentile exceeds 0.95.

Figures 17 a and c show the worst-performing topologies of the L-bracket, optimized for a design load of 500 kN, for damage percentiles 0 and 1, respectively. The best-performing design (Figure 17 b) is achieved for a damage percentile of 0.95 and has a material volume which is almost identical to that of the fully nonlinearly optimized design. Although a damage percentile of 0.95 leads to the best results for this example, we assume a more conservative value of 0.9 for the damage percentile P_d for the following cases, to avoid sub-optimal results due to an excessively high damage percentile.

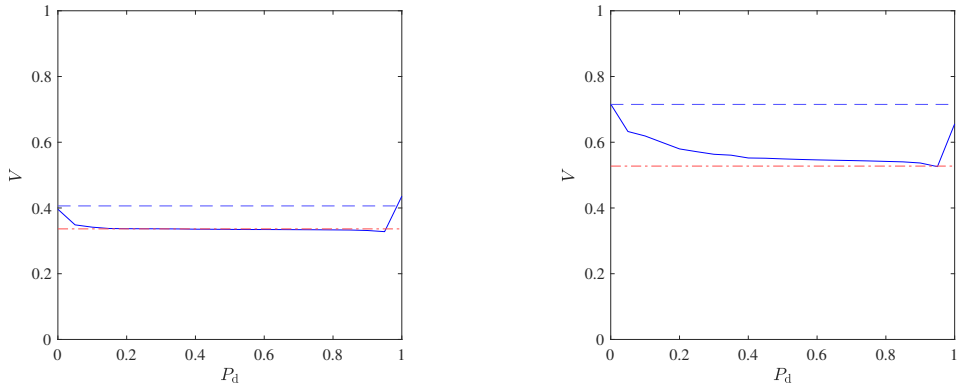

(a) Design load: 300 kN **(b)** Design load: 500 kN

FIGURE 16 Influence of the damage percentile on the volume fraction of the optimized design. The blue dashed line represents the volume fraction of a structure optimized with the simplified optimization strategy, but with the elastic compliance C instead of the one-step compliance C_d. The red dash-dot line shows the volume fraction of a design optimized with the fully nonlinear optimization strategy.

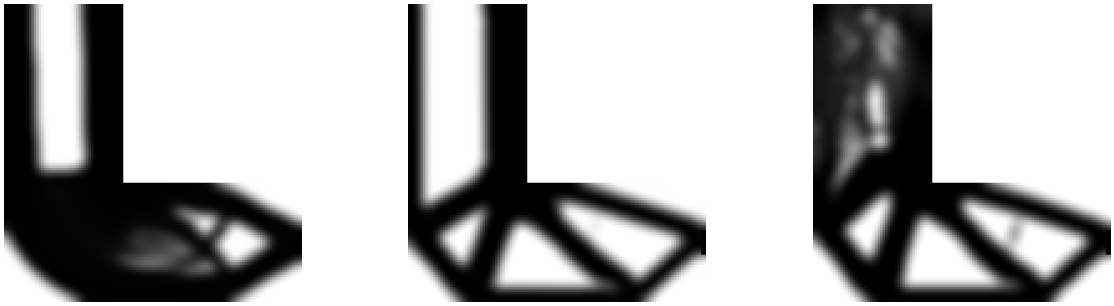

(a) $P_d = 0$ **(b)** $P_d = 0.95$ **(c)** $P_d = 1$

FIGURE 17 Topology of the L-bracket, optimized with the simplified strategy for a design load of 500 kN, with different values of the damage percentile.

3.3 | Length scale control

To increase the discrete character of the optimized designs, and to impose a minimal length scale on the solid and void regions, the robust projection method by Wang[21] is applied. This method uses a Heaviside projection function to project the element densities $\tilde{\boldsymbol{\rho}}$ to values which are closer to zero or one. In its discrete form, the used Heaviside function projects values below threshold η_H to zero, and values larger than the threshold to one. The discrete function is replaced by a smooth, differentiable Heaviside function, which transforms an element density $\tilde{\rho}_e$ to a projected density $\bar{\tilde{\rho}}_e$, to enable the use of a gradient-based optimization algorithm:

$$\bar{\tilde{\rho}}_e = \frac{\tanh(\beta_H \eta_H) + \tanh(\beta_H(\tilde{\rho}_e - \eta_H))}{\tanh(\beta_H \eta_H) + \tanh(\beta_H(1 - \eta_H))} \tag{41}$$

where the projection sharpness β_H describes the level of smoothness. The smooth Heaviside function (41) approaches the discrete function for a projection sharpness β_H going to infinity.

For the robust projection method[21], the element densities $\tilde{\rho}_e$ are projected using the Heaviside function (41) with three different values of the threshold η_H. The design is eroded for a threshold η_H higher than 0.5, whereas a lower value of the threshold leads to a dilated design. The projected design with threshold η_H equal to 0.5 generates the intermediate densities, which are

used as a blueprint for production. The structural analysis is performed using the eroded design, and the minimization of material volume is based on the dilated design, guaranteeing a minimal length scale of the solid and void regions of the design.

For both optimization strategies, the projection sharpness β_{H} of the Heaviside filter is increased by a factor 2 every 50 iterations of the inner loop, starting at 1 and with a maximal value of 8, which gradually increases the discreteness of the design during the optimization. The projection sharpness is kept relatively low to increase the stability of the convergence. The threshold $\eta_{\mathrm{H}}^{\mathrm{d}}$ for the dilated design is chosen as 0.25, and threshold $\eta_{\mathrm{H}}^{\mathrm{e}}$ for the eroded design is 0.75. Combining a filter radius r of 0.25 m with these threshold values leads to a minimal length scale of 0.25 m in the intermediate design [1].

The optimization problem of equation (29) is reformulated as:

$$\begin{aligned} \min_{\boldsymbol{\rho}} :\quad & V^{\mathrm{d}} = \frac{\sum_e v_e \tilde{\bar{\rho}}_e^{\mathrm{d}}}{\sum_e v_e} \\ \text{s.t.} :\quad & f_{\mathrm{r}}^{\mathrm{e}} \geq f_{\mathrm{d}} \\ & 0 \leq \rho_e \leq 1 \end{aligned} \tag{42}$$

where $\tilde{\bar{\rho}}_e^{\mathrm{d}}$ is the dilated projected density of element e, V^{d} is the volume fraction of the dilated design, and $f_{\mathrm{r}}^{\mathrm{e}}$ is the load resistance of the eroded design. For all presented cases, the intermediate and dilated designs have a higher load resistance than the eroded design. The constraint on the eroded design therefore suffices to ensure a minimal length scale.

The L-bracket is optimized again for a design load of 500 kN, using both optimization strategies in combination with the robust projection method [21]. The resulting intermediate designs are shown in Figures 18 a and b, and Figure 19 shows the load-displacement curves of the eroded, intermediate and dilated designs. The load-displacement curves show that the load resistance of the eroded designs correspond to the design load. The volume fraction and computation time are shown in Table 4. When comparing these results, the optimized volume fractions are very similar, with the simplified optimization strategy leading to an intermediate design which is 0.7% heavier. The total computation time of the fully nonlinear optimization is 3 hours and 43 minutes, which is 8.9 times longer than the simplified optimization, which lasted 25 minutes. For the intermediate designs shown in Figures 18 a and b, the measures of non-discreteness, as defined by Sigmund [27], are 0.084 and 0.077, respectively.

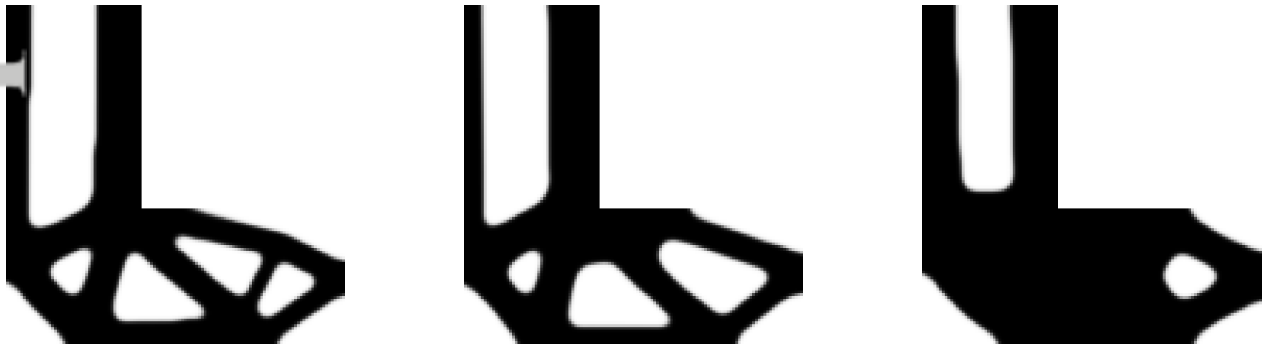

(a) Fully nonlinear $V^{\mathrm{i}} = 0.578$

(b) Simplified ($P_{\mathrm{d}} = 0.9$) $V^{\mathrm{i}} = 0.582$

(c) Simplified elastic $V^{\mathrm{i}} = 0.755$

FIGURE 18 Intermediate design of the L-bracket, optimized with the fully nonlinear, simplified, and simplified elastic strategy, in combination with the robust projection method [21].

[1] Figure 12 in the paper by Wang et al. [21] shows the length scale on the intermediate design in function of the threshold η. Note that the values of the y-axis should be divided by two in order to be correct.

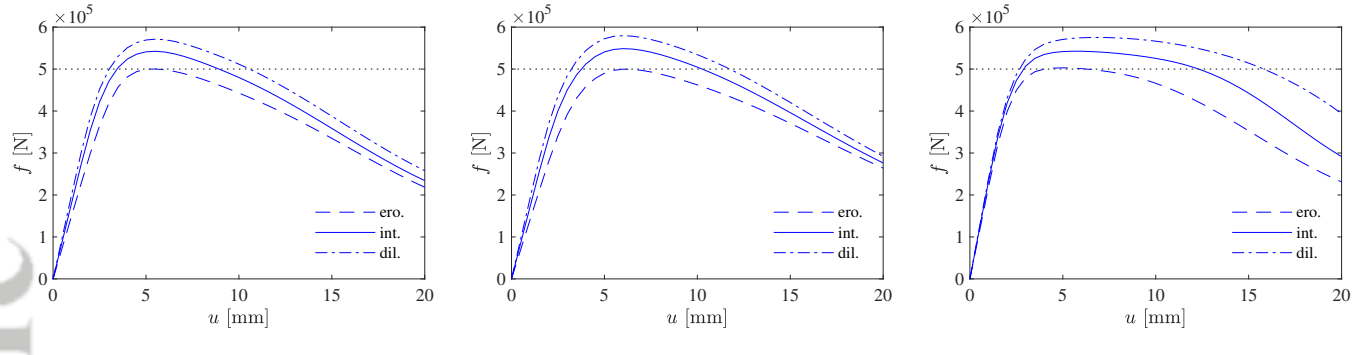

(a) Fully nonlinear **(b)** Simplified (Pd = 0.9) **(c)** Simplified elastic

FIGURE 19 Load-displacement curves of the L-bracket, optimized with the fully nonlinear, simplified, and simplified elastic strategy, computed for the eroded, intermediate, and dilated design. The dotted line represents the design load.

TABLE 4 Comparison of the fully nonlinear and simplified optimization strategy for the L-bracket, using the robust projection method[21].

	Fully nonlinear	**Simplified**	
		$P_\mathrm{d} = 0.9$	Elastic
Volume fraction			
– Dilated	0.664	0.661	0.801
– Intermediate	0.578	0.582	0.755
– Eroded	0.483	0.495	0.704
Computation time (hh:mm:ss)			
– Optimization loop	03:26:22	00:05:30	00:03:12
– Nonlinear simulation	00:16:19	00:19:37	00:16:24
– Total	03:42:41	00:25:07	00:19:37

We optimize the L-bracket again for a design load of 500 kN, but with the elastic compliance C instead of the one-step compliance C_d. Figure 18 c shows the elastically optimized topology, and Figure 19 c shows the corresponding load-displacement curves. With an intermediate volume fraction of 0.755, the simplified elastic result is 30% heavier than the designs optimized with the fully nonlinear strategy and the simplified optimization strategy.

3.4 | Convergence

To compare the fully nonlinear strategy with the simplified optimization strategy with a damage percentile of 0.9, we consider the convergence of several parameters during the optimization of the L-bracket example. Figures 20 a and b show the convergence of the objective function, the dilated volume fraction, at each design iteration i. The projection sharpness β is updated after 50, 100, and 150 iterations, leading to jumps in the volume fraction. During the second half of the optimization, the projection parameters remain constant, to allow for the design to converge to its local optimum.

Figures 20 c and d show the evolution of the structure's load resistance f_r, which is computed every 25 iterations. Since both optimizations start from a solid design, the initial load resistance is identical. The load resistance converges to the design load of 500 kN with both optimization strategies.

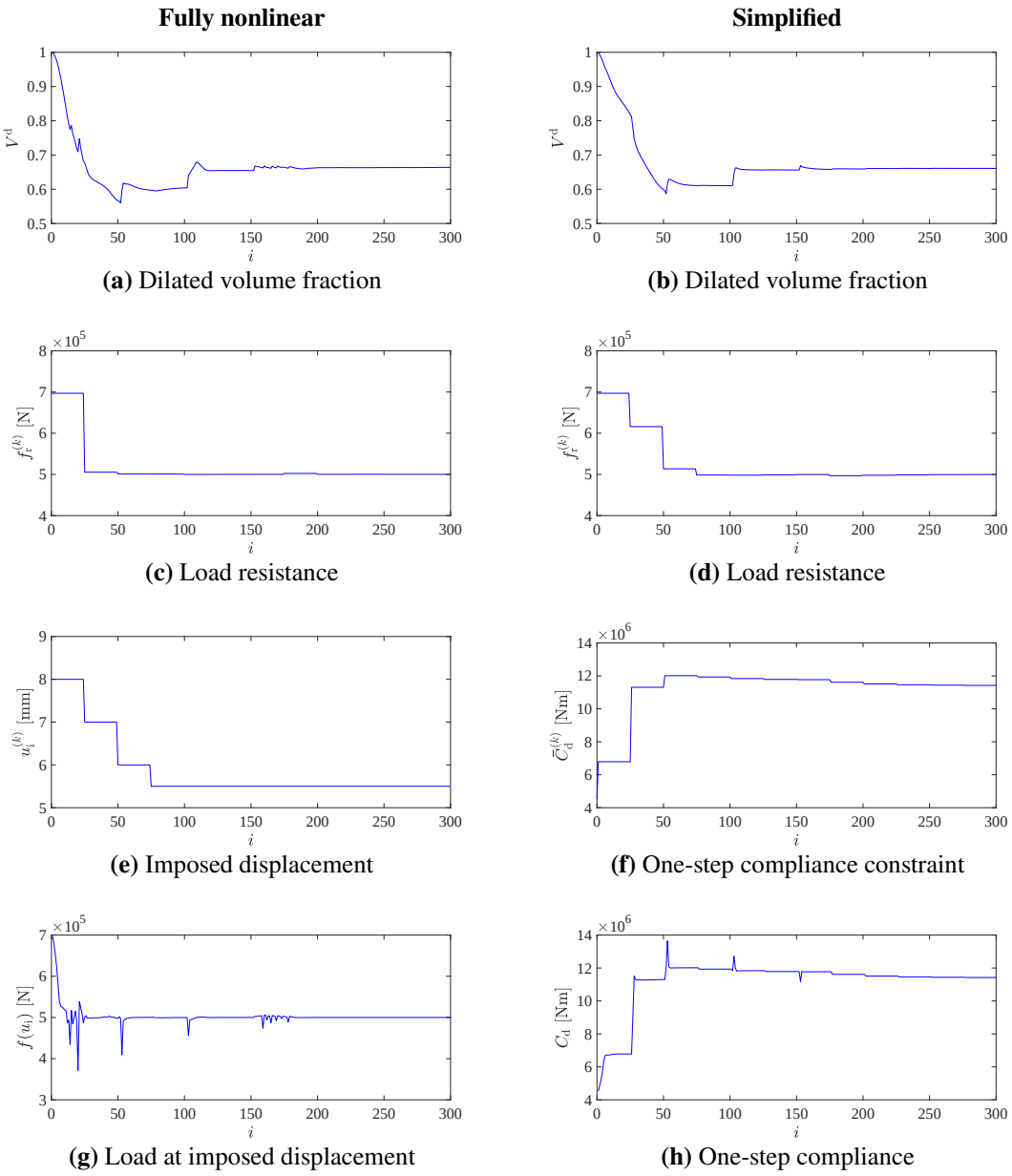

(a) Dilated volume fraction **(b)** Dilated volume fraction

(c) Load resistance **(d)** Load resistance

(e) Imposed displacement **(f)** One-step compliance constraint

(g) Load at imposed displacement **(h)** One-step compliance

FIGURE 20 Convergence of different parameters for the L-bracket optimization, using the fully nonlinear strategy, and the simplified optimization strategy with a damage percentile P_{d} of 0.9.

A parameter update is performed every 25 iterations. The imposed displacement u_{i} is updated for the fully nonlinear optimization strategy, and the compliance constraint $\bar{C}_{\mathrm{d}}$ is updated for the simplified optimization strategy. The imposed displacement can only be updated in discrete steps, because the load-displacement curve is only constructed for steps of a predefined size Δu_{ld}, which is equal to 0.5 mm for the L-bracket example. Therefore, the imposed displacement in Figure 20 e is always a multiple of 0.5. Reducing the displacement step size Δu_{ld} would further increase the accuracy, but at the cost of additional computation time. For the simplified optimization strategy, the compliance constraint $\bar{C}_{\mathrm{d}}$ is adapted at every parameter update, as can be seen in Figure 20 f. Since the compliance constraint is not updated in discrete steps of a fixed size, but continuously, the convergence is more gradual and stable, compared to the fully nonlinear method.

The convergence of the constraint function is shown in Figures 20 g and h. For the fully nonlinear strategy, the load f at the imposed displacement u_{i} must be higher than or equal to the design load. For the simplified strategy, the compliance C_{d} must

remain lower than or equal to the compliance constraint.

Overall, the convergence graphs in Figure 20 show a more smooth convergence for the simplified optimization strategy than for the fully nonlinear strategy. Because of the less smooth convergence, the fully nonlinear optimization strategy is more sensitive to the choice of optimization parameters, such as the continuation scheme for the projection sharpness β_{H}.

3.5 | Stress concentration at re-entrant corner

It can be observed that all optimized topologies in Figure 18 have a sharp re-entrant corner, as opposed to the typical rounded corner of an L-bracket optimized with a stress constraint. This may seem counter-intuitive, because the sharp corner leads to a stress concentration, which leads to an early initiation of damage at that location. However, while avoiding stress concentrations can effectively delay the onset of damage in a structure, the load-bearing capacity of a structure is determined by the entire damage history during loading. Instead of avoiding stress concentrations, the optimizer typically adds material in all regions where damage will arise.

To verify that a design with a rounded re-entrant corner is less material efficient, we solve the L-bracket optimization problem again, but with an enforced rounded corner. To accomplish this, the design variables $\boldsymbol{\rho}$ are fixed at a value of zero in a circular region with its center at 25 cm to the right of the re-entrant corner, and with a radius of 25 cm. Note that this will only lead to a perfectly rounded corner for the eroded design, which is used for the computation of the load resistance during optimization. The topologies obtained with the fully nonlinear and simplified optimization strategy are shown in Figure 21. By rounding the re-entrant corner, the material use increases with 8.3% for the fully nonlinear strategy, and 14.9% for the simplified strategy, for the same load-bearing capacity as the designs with a sharp corner. The corresponding load-displacement curves are shown in Figure 22.

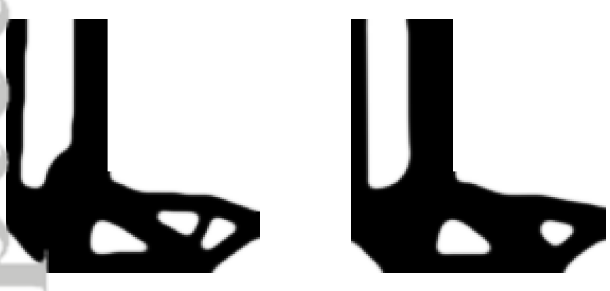

(a) Fully nonlinear $V^{\mathrm{i}} = 0.626$ **(b)** Simplified ($P_{\mathrm{d}} = 0.9$) $V^{\mathrm{i}} = 0.669$

FIGURE 21 Intermediate design of the L-bracket, optimized with the fully nonlinear and simplified strategy, with an enforced rounding of the re-entrant corner.

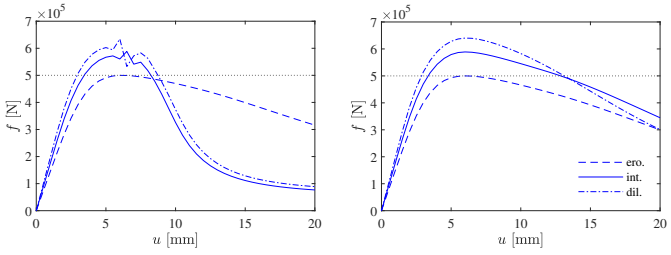

(a) Fully nonlinear $V^{\mathrm{i}} = 0.626$ **(b)** Simplified ($P_{\mathrm{d}} = 0.9$) $V^{\mathrm{i}} = 0.669$

FIGURE 22 Load-displacement curves of the L-bracket, optimized with the fully nonlinear and simplified strategy, computed for the eroded, intermediate, and dilated design.

3.6 | Influence of design load on volume fraction

We assess the influence of the design load on the volume fraction of optimized designs, by performing the L-bracket optimization as described in Section 3.3 for a design load ranging from 100 tot 600 kN, in steps of 100 kN. As expected, a higher design load leads to a higher volume fraction. While the fully nonlinear optimization strategy leads to the most material efficient designs for a design load of 400 to 600 kN, the designs obtained for a design load of 100 to 300 kN are clearly local minima and in this particular case, the simplified optimization method actually turns out to lead to more material efficient designs for these particular design loads.

Figure 24 shows the intermediate topologies of the optimized designs. The designs optimized with the simplified optimization strategy have very similar topologies, with only a variation of the thickness of the solid regions, whereas the fully nonlinearly optimized designs show a greater variation, at least for the ill-converged designs for a design load of 100 and 200 kN. More refined continuation and optimization strategies could be investigated to mitigate convergence to local minima, but are not pursued further for now.

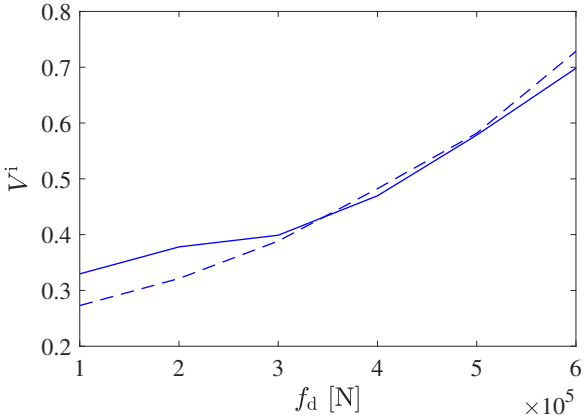

FIGURE 23 Influence of the design load f_{d} on the intermediate volume fraction V^{i} of the optimized L-bracket. The solid line represents the fully nonlinear optimization strategy, and the dashed line represents the simplified strategy.

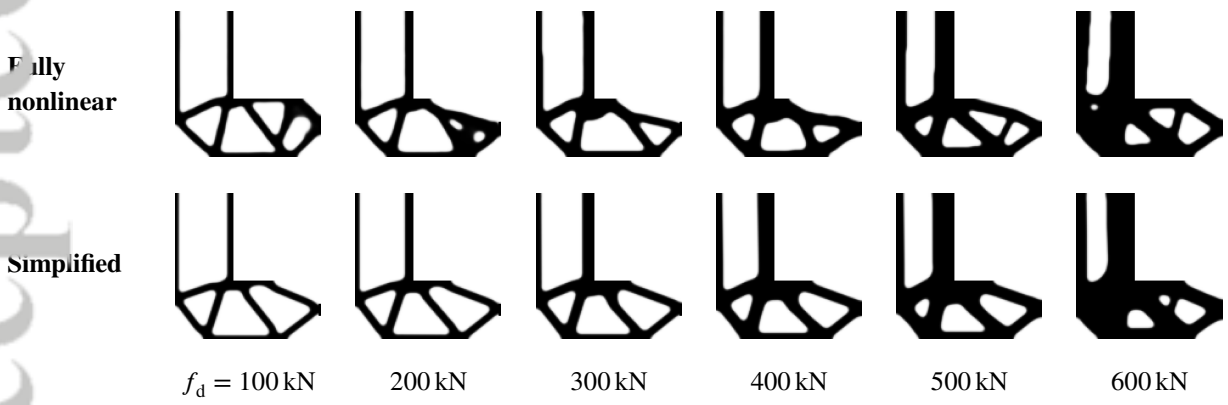

FIGURE 24 Intermediate design of the L-bracket, optimized with the fully nonlinear and simplified strategy, for different design loads f_{d}.

4 | ADDITIONAL CASE STUDIES

Supplementary to the previously discussed L-bracket case study, two additional case studies are introduced, to compare the fully nonlinear and simplified optimization strategies. For this article, we only consider two-dimensional structures to avoid the excessive computation time associated with three-dimensional problems. Both strategies are compared in terms of computation time, material volume, and topology of the optimized designs. Table 5 shows the different parameters that are used for the additional cases. The in-plane thickness of all structures is 1 meter, and plane stress is assumed. The robust projection method[21],

as described in Section 3.3, is used for all following case studies. We use a damage percentile P_d of 0.9 for the simplified optimization strategy. In Section 4.3, the optimality of the chosen damage percentile is verified for all case studies.

TABLE 5 Material and optimization parameters for the clamped beam and the cantilever beam.

α	β	k	c_s	l_c [m]	E_0 [MPa]	E_{min} [MPa]	ν	κ_0	r [m]
.95	100	5	5	0.3	30×10^3	30×10^{-6}	0.2	1×10^{-4}	0.5

.1 | Clamped beam

We consider a beam which is clamped on both sides and loaded in the middle. The beam measures 20 by 5 meters. Because we assume a symmetric damage scenario, the beam can be simulated by modeling half of the structure and adding symmetry boundary conditions (see Figure 25). The model consists of 100 by 50 finite elements and the beam is designed to support a load of 6000 kN, half of which is distributed along 6 nodes of the finite element model, as shown in the detail in Figure 25. The displacement step size Δu_{ld}, used for the computation of the load-displacement curve, is 1 mm. The clamped beam allows for testing the optimization of damage-resistant structures when no stress concentrations exist in the solid structure. In this case, the position where damage initiates depends only on the optimized topology.

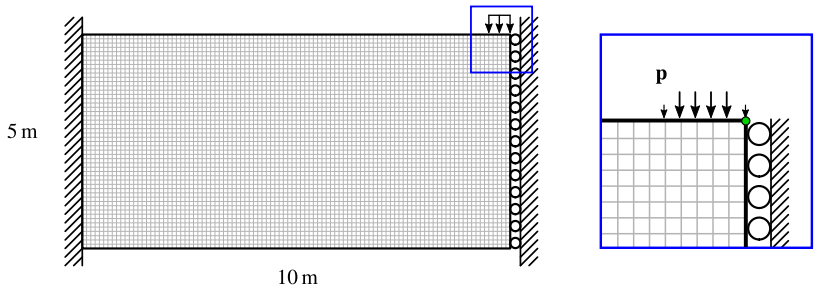

FIGURE 25 Dimensions and boundary conditions of the half clamped beam model. The detail shows the position of the loads and the green dot highlights the displacement-control DOF.

Figures 26 a and b show the topology of the designs optimized with the fully nonlinear and simplified optimization strategy respectively, and the corresponding load-displacement curves are shown in Figure 27. The volume fractions and computation time are summarized in Table 6. With an intermediate volume fraction of 0.325, the resulting design of the simplified optimization is 11% heavier than the fully nonlinearly optimized design, which has an intermediate volume fraction of 0.293. The total computation time with the fully nonlinear strategy is 2 hours and 9 minutes, which is 11 times longer than the simplified optimization method, which lasted 11 minutes and 40 seconds.

Figures 26 c and 27 c show the topology and load-displacement curves of a design optimized with the simplified elastic optimization strategy, which uses the elastic compliance instead of the one-step compliance. While the elastically optimized design also fulfills the constraint of the load-resistance, the structure is 213% heavier than the fully nonlinear design and 192% heavier than the simplified design with one-step damage.

It can be noted that the load-displacement curve of the eroded, fully nonlinear design (Figure 26 a) is rather unexpected, since it suggests that – for large displacements – the eroded design can withstand higher loads than the intermediate and

(a) Fully nonlinear $V^{\mathrm{i}} = 0.293$ | **(b)** Simplified ($P_{\mathrm{d}} = 0.9$) $V^{\mathrm{i}} = 0.325$ | **(c)** Simplified elastic $V^{\mathrm{i}} = 0.624$

FIGURE 26 Intermediate design of the clamped beam, optimized with the fully nonlinear, simplified, and simplified elastic strategies.

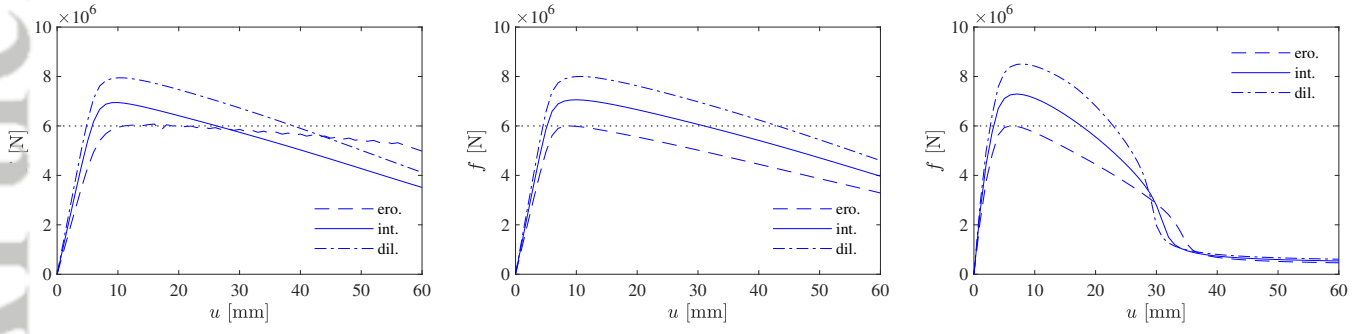

(a) Fully nonlinear | **(b)** Simplified ($P_{\mathrm{d}} = 0.9$) | **(c)** Simplified elastic

FIGURE 27 Load-displacement curves of the clamped beam, optimized with the fully nonlinear, simplified, and simplified elastic strategy, computed for the eroded, intermediate, and dilated design.

dilated designs. This is most likely a numerical artefact, rather than a physically meaningful result, since the Newton-Raphson solver has difficulty converging between the 15th and 56th displacement step. For approximately half of the displacement steps in this range, the solver fails to converge within 20 iterations, which also explains the slightly oscillating trajectory of the load-displacement curve between 15 and 56 mm. Since the 'tail' of the load-displacement curve is not considered during the optimization, the obtained results are not affected.

While the one-step damage model of the simplified optimization strategy only captures first-order effects of damage, it performs very well compared to the simplified elastic optimization. Both the fully nonlinear and simplified optimization strategy lead to structures which work mainly in compression. Since the elastic compliance does not reflect any difference in material behavior in tension and compression, the elastically optimized topology (Figure 26 c) combines compressive trusses – similar to the topologies in Figures 26 a and b – with tensile elements, which follow a cable-like trajectory. Because the considered material is weak in tension, these tensile elements drastically increase the material volume, without a significant contribution to the load resistance of the structure.

4.2 | Cantilever beam (multiple load cases)

The final case consists of a cantilever beam, measuring 24 by 6 meters, modeled by 240 by 60 finite elements. The beam is supported at the bottom left corner and at two thirds of the total length (see Figure 28). The supports of the structure are modeled as roller supports, each distributed over a length of 1 m. The bottom left node of the structure is restrained horizontally, to prevent rigid body motion. The example of the cantilever beam has been chosen to demonstrate the optimization of a structure with multiple load cases, as the weight of the structure is minimized, while requiring to withstand two different load scenarios without failing. For the first load case, the load f_1 is applied in the middle of the main span, distributed according to the load distribution vector $\mathbf{p}_1$. In the second load case, the load f_2 is applied on the end of the cantilever, distributed according to the load distribution vector $\mathbf{p}_2$. The spatial load distribution for both load cases is shown on the right-hand side of Figure 28. Each

TABLE 6 Comparison of the fully nonlinear and simplified optimization strategy for the clamped beam and cantilever beam.

	Clamped beam			Cantilever beam		
	Nonlinear	Simplified		Nonlinear	Simplified	
		$P_d = 0.9$	Elastic		$P_d = 0.9$	Elastic
Volume fraction						
– Dilated	0.349	0.375	0.702	0.665	0.711	0.778
– Intermediate	0.293	0.325	0.624	0.610	0.646	0.734
– Eroded	0.236	0.272	0.537	0.551	0.572	0.682
Computation time (hh:mm:ss)						
– Optimization loop	01:58:56	00:02:38	00:01:50	17:53:49	00:07:58	00:03:51
– Load-displacement curves	00:10:30	00:09:01	00:09:00	01:24:22	00:57:06	00:47:14
– Total	02:09:26	00:11:40	00:10:50	19:18:11	01:05:05	00:51:06

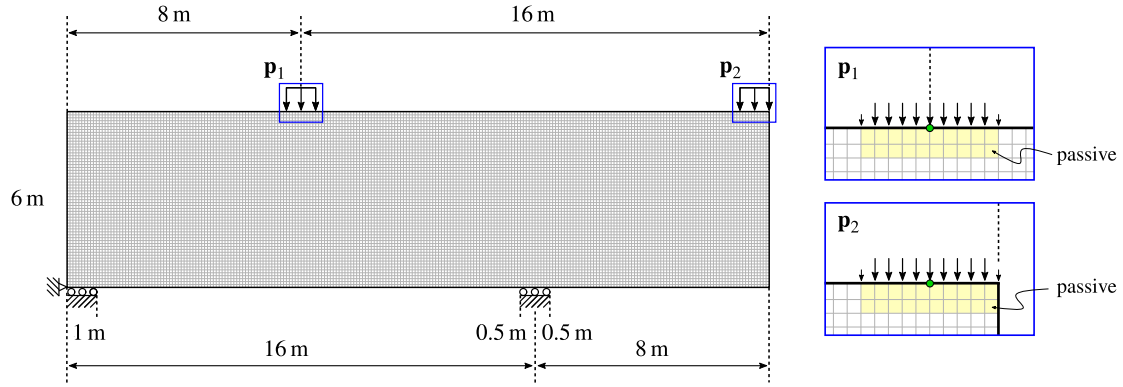

FIGURE 28 Dimensions and boundary conditions of the cantilever beam. Vectors $\mathbf{p}_1$ and $\mathbf{p}_2$ show the load distribution for each load case. The green dots represent the displacement-control DOFs for the different load cases.

load is distributed over 11 nodes, with the first and last node carrying only half of the force on the other nodes. Each load case corresponds with a different displacement-control DOF, the vertical displacement of the nodes highlighted in green in the details of Figure 28. The displacement step size Δu_{ld} is equal to 0.25 mm for the first load case, and 0.5 mm for the second load case. The passive elements, highlighted in Figure 28, have a fixed density of 1 during the optimization process.

The cantilever beam is optimized to withstand a design load f_d of 3000 kN for both load cases. The optimization problem (42) is reformulated as follows, to consider both load cases:

$$\begin{aligned} \min_{\boldsymbol{\rho}} :\quad & V^{\text{d}} = \frac{\sum_e v_e \tilde{\bar{\rho}}_e^{\text{d}}}{\sum_e v_e} \\ \text{s.t.} :\quad & f_{\text{r},j}^{\text{e}} \geq f_{\text{d},j} \qquad j = 1, 2 \\ & 0 \leq \rho_e \leq 1 \end{aligned} \tag{43}$$

where the load resistance $f_{\text{r},j}^{\text{e}}$ for each load case j must be larger than or equal to the design load $f_{\text{d},j}$ for that load case. Each load case also requires the construction of its respective load-displacement curve, and the parameter updates must now be performed for each individual load case.

Figures 29 a and b show the topology of the designs optimized with the fully nonlinear and simplified optimization strategy respectively, and the corresponding load-displacement curves are shown in Figure 30. Table 6 summarizes the volume fractions

and computation time. With an intermediate volume fraction of 0.646, the design optimized with the simplified strategy is 5.9% heavier than the fully nonlinearly optimized design, which has an intermediate volume fraction of 0.610. The total computation time of the fully nonlinear optimization strategy is 19 hours and 18 minutes, and the simplified strategy lasted only 1 hour and 5 minutes, making it 17.8 times faster.

(a) Fully nonlinear $V^{\mathrm{i}} = 0.610$ **(b)** Simplified ($P_{\mathrm{d}} = 0.9$) $V^{\mathrm{i}} = 0.646$ **(c)** Simplified elastic $V^{\mathrm{i}} = 0.734$

FIGURE 29 Intermediate design of the clamped beam, optimized with the fully nonlinear, simplified, and simplified elastic strategy.

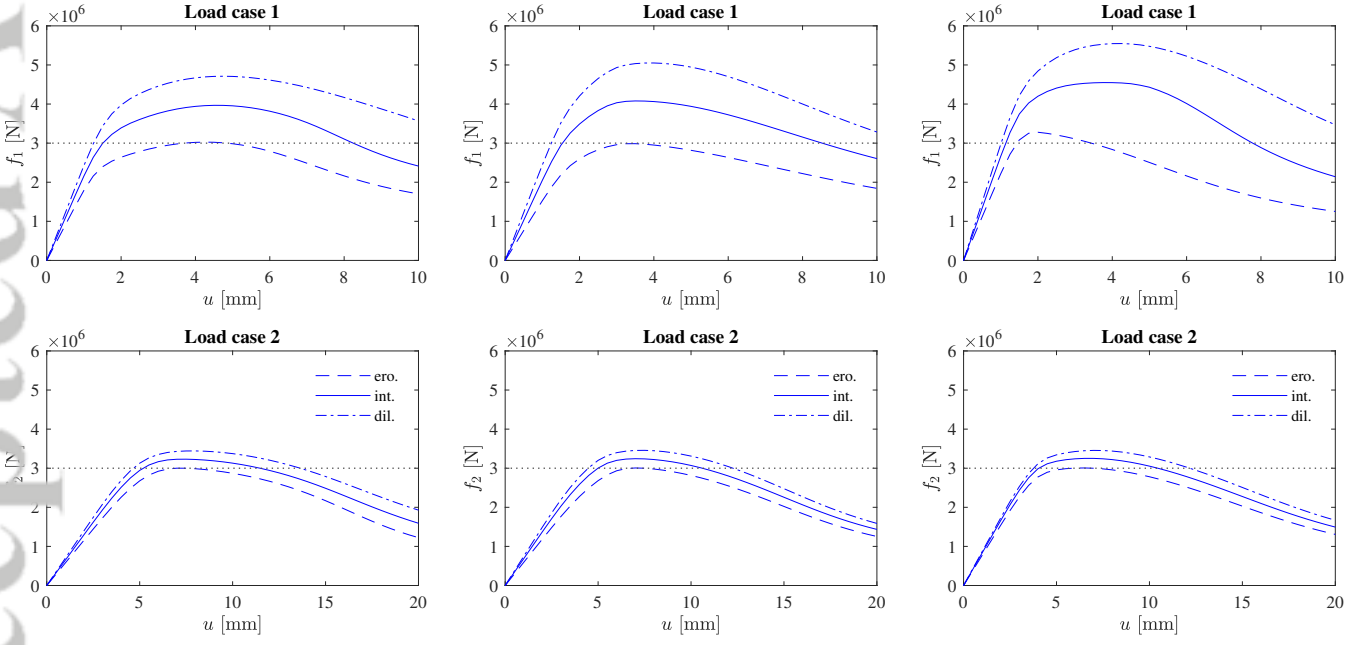

(a) Fully nonlinear **(b)** Simplified ($P_{\mathrm{d}} = 0.9$) **(c)** Simplified elastic

FIGURE 30 Load-displacement curves of the clamped beam, optimized with the fully nonlinear, simplified, and simplified elastic strategy, computed for the eroded, intermediate, and dilated design for both load cases.

We optimize the cantilever beam again, but now with the simplified elastic strategy. The topology and load-displacement curves of the optimized design are shown in Figures 29 c and 30 c. With an intermediate volume fraction of 0.734, the elastically optimized design is 20.3% heavier than the fully nonlinear design, and 13.6% heavier than the simplified design.

4.3 | Verification of the optimal damage percentile

With the simplified optimization strategy, the choice of the damage percentile P_{d} defines the performance of the optimized design. We assumed a value of 0.9 for the damage percentile for all test cases in combination with the robust projection

method[21]. To verify if this value of the damage percentile leads to well-performing designs, we repeat the optimizations for a range of values for the damage percentile between 0 and 1. Figure 31 shows the intermediate volume fraction of the optimized design for each value of the damage percentile.

For the L-bracket, the results are very similar to the results in Section 3.2.2, with increasing values of the damage percentile leading to designs with lower volume fractions, except for a damage percentile higher than 0.95. For values close to 0 and 1, the volume fraction is similar to that of the elastically optimized L-bracket (blue dashed line). For a damage percentile of 0.95, the simplified optimization algorithm even outperforms the fully nonlinear optimization strategy in terms of material efficiency. This could be explained by the severe non-convexity of the optimization problem, making it a non-trivial task to find the global optimum. For the clamped beam, any value of the damage percentile between 0.15 and 1 leads to a very similar optimized volume fraction, which is slightly higher than the volume fraction of the fully nonlinearly optimized clamped beam. The pattern is less clear for the case study of the cantilever beam. As for the other examples, very low values of the damage percentile lead to a volume fraction close to that of the elastically optimized design. For a damage percentile around 0.2, the volume fraction is close to that of the fully nonlinearly optimized design. For higher values of the damage percentile, the intermediate volume fraction fluctuates between 0.604 and 0.653.

This test shows that for the L-bracket and the clamped beam, any value of the damage percentile between 0.5 and 0.95 would have given very similar results in terms of material efficiency. For the cantilever beam, the optimal value of the damage percentile would be between 0.2 and 0.35, or close to 0.6. In the absence of a clear pattern, we cannot advise a generally applicable optimal value of the damage percentile, but based on these three tests we can assume that values of the damage percentile between 0.2 and 0.95 lead to relatively similar material efficiency of the optimized designs. We can also conclude that, for all presented cases, the simplified optimization strategy with one-step compliance outperforms the simplified elastic optimization strategy, as long as the damage percentile is less than 1.

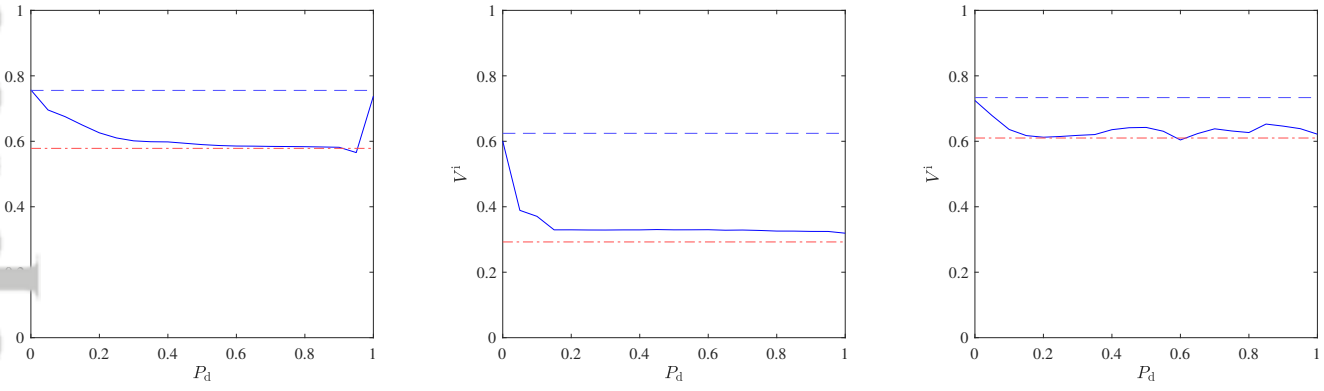

(a) L-bracket **(b)** Clamped beam **(c)** Cantilever beam

FIGURE 31 Influence of the damage percentile on the intermediate volume fraction of the optimized design of the different case studies, using the simplified optimization strategy in combination with the robust projection method[21]. The blue dashed line represents the volume fraction of an elastically optimized structure. The red dash-dot line shows the volume fraction of a fully nonlinearly optimized structure.

5 | CONCLUSION

Several methods exist to maximize the damage-resistance of topology optimized structures, using nonlinear models for the simulation of damage. However, no method exists yet to solve the typical engineering problem of minimizing a structure's weight while guaranteeing a predefined load capacity, considering the softening behavior of quasi-brittle materials. This article

suggests two optimization strategies: a fully nonlinear strategy and a simplified strategy.

In the fully nonlinear optimization strategy, the optimization problem is formulated as a minimal weight problem, with a constraint that requires the load corresponding to a certain imposed displacement to be larger than or equal to the design load. To ensure that the load at the imposed displacement corresponds to the peak of the load-displacement curve, the imposed displacement is modified at regular intervals throughout the optimization procedure. A nonlinear damage model is used for computing the load-displacement curve and the load corresponding with the imposed displacement.

The simplified optimization strategy uses a novel simplified damage model, which computes damage in a single step. This simplified damage model is used to determine the so-called one-step compliance, which is a first-order estimate of the compliance of the damaged structure. The optimization problem is formulated as a minimum weight problem with a constraint on the one-step compliance. To control the accuracy of the solution, the load-displacement curve is computed occasionally, using a nonlinear damage model. Depending on the computed load capacity, the one-step compliance constraint is either tightened or relaxed.

Three case studies are presented to test the feasibility of both optimization strategies and to compare the optimized results. For all three cases, the optimization strategies effectively lead to structures with a load capacity almost identical to the design load. Regarding computation time, the simplified strategy is 8 to 18 times faster than the fully nonlinear strategy, at the expense of a lower material efficiency: the simplified optimization strategy leads to designs which require between 0.7% and 13% more material than the designs optimized with the fully nonlinear optimization strategy for the same load capacity.

ACKNOWLEDGMENTS

We want to express our gratitude to the Foundation for Scientific Research - Flanders (FWO) for funding this research through a Strategic Basic Research grant (1S92920N), as well as a travel grant (V417620N) for a stay at the Technical University of Denmark (DTU), under supervision of professor Ole Sigmund. This work was performed partially within the frame of the project C16/17/008 "Efficient methods for large-scale PDE-constrained optimization in the presence of uncertainty and complex technological constraints" funded by the Research Council of KU Leuven. On behalf of professor Ole Sigmund, we also want to thank the Villum foundation for their contribution through the Villum investigator project 'InnoTop'.

APPENDIX: SENSITIVITY ANALYSIS

For the simplified optimization strategy, as described in Section 3.2.2, the one-step compliance is differentiated with respect to the design variables $\boldsymbol{\rho}$:

$$\frac{\mathrm{d}C_\mathrm{d}}{\mathrm{d}\boldsymbol{\rho}} = \frac{\mathrm{d}}{\mathrm{d}\boldsymbol{\rho}}\left(\mathbf{f}_\mathrm{os}^\mathrm{T}\mathbf{u}_\mathrm{d}\right) \tag{44}$$

When using a density filter, or the robust projection method[21], the design variables $\boldsymbol{\rho}$ should be replaced by the element densities $\tilde{\boldsymbol{\rho}}$ or projected densities $\bar{\tilde{\boldsymbol{\rho}}}$, respectively.

Based on the equilibrium equations (21) and (22), an adjoint sensitivity analysis is performed, with one adjoint vector $\boldsymbol{\lambda}_i$ per equilibrium:

$$C_\mathrm{d} = \mathbf{f}_\mathrm{os}^\mathrm{T}\mathbf{u}_\mathrm{d} + \boldsymbol{\lambda}_1^\mathrm{T}\left[\mathbf{f}_\mathrm{os} - \mathbf{K}\mathbf{u}\right] + \boldsymbol{\lambda}_2^\mathrm{T}\left[\mathbf{f}_\mathrm{os} - \mathbf{K}_\mathrm{d}(\mathbf{u})\,\mathbf{u}_\mathrm{d}\right] \tag{45}$$

Note the direct dependency of $\mathbf{K}_\mathrm{d}$ on both $\mathbf{u}$ and $\boldsymbol{\rho}$:

$$\frac{\mathrm{d}C_\mathrm{d}}{\mathrm{d}\boldsymbol{\rho}} = \mathbf{f}_\mathrm{os}^\mathrm{T}\frac{\mathrm{d}\mathbf{u}_\mathrm{d}}{\mathrm{d}\boldsymbol{\rho}} + \boldsymbol{\lambda}_1^\mathrm{T}\left[-\frac{\partial\mathbf{K}}{\partial\boldsymbol{\rho}}\mathbf{u} - \mathbf{K}\frac{\mathrm{d}\mathbf{u}}{\mathrm{d}\boldsymbol{\rho}}\right] + \boldsymbol{\lambda}_2^\mathrm{T}\left[-\left(\frac{\partial\mathbf{K}_\mathrm{d}}{\partial\mathbf{u}}\frac{\mathrm{d}\mathbf{u}}{\mathrm{d}\boldsymbol{\rho}} + \frac{\partial\mathbf{K}_\mathrm{d}}{\partial\boldsymbol{\rho}}\right)\mathbf{u}_\mathrm{d} - \mathbf{K}_\mathrm{d}(\mathbf{u})\frac{\mathrm{d}\mathbf{u}_\mathrm{d}}{\mathrm{d}\boldsymbol{\rho}}\right] \tag{46}$$

This can be further elaborated to obtain:

$$\frac{\mathrm{d}C_\mathrm{d}}{\mathrm{d}\boldsymbol{\rho}} = -\boldsymbol{\lambda}_1^\mathrm{T}\frac{\partial\mathbf{K}}{\partial\boldsymbol{\rho}}\mathbf{u} - \boldsymbol{\lambda}_2^\mathrm{T}\frac{\partial\mathbf{K}_\mathrm{d}}{\partial\boldsymbol{\rho}}\mathbf{u}_\mathrm{d} - \boldsymbol{\lambda}_1^\mathrm{T}\mathbf{K}\frac{\mathrm{d}\mathbf{u}}{\mathrm{d}\boldsymbol{\rho}} - \boldsymbol{\lambda}_2^\mathrm{T}\frac{\partial\mathbf{K}_\mathrm{d}}{\partial\mathbf{u}}\frac{\mathrm{d}\mathbf{u}}{\mathrm{d}\boldsymbol{\rho}}\mathbf{u}_\mathrm{d} + \mathbf{f}_\mathrm{os}^\mathrm{T}\frac{\mathrm{d}\mathbf{u}_\mathrm{d}}{\mathrm{d}\boldsymbol{\rho}} - \boldsymbol{\lambda}_2^\mathrm{T}\mathbf{K}_\mathrm{d}(\mathbf{u})\frac{\mathrm{d}\mathbf{u}_\mathrm{d}}{\mathrm{d}\boldsymbol{\rho}} \tag{47}$$

Rearrange to combine all terms containing the derivatives $\frac{\mathrm{d}\mathbf{u}}{\mathrm{d}\boldsymbol{\rho}}$ and $\frac{\mathrm{d}\mathbf{u}_\mathrm{d}}{\mathrm{d}\boldsymbol{\rho}}$:

$$\frac{\mathrm{d}C_\mathrm{d}}{\mathrm{d}\boldsymbol{\rho}} = -\boldsymbol{\lambda}_1^\mathrm{T}\frac{\partial\mathbf{K}}{\partial\boldsymbol{\rho}}\mathbf{u} - \boldsymbol{\lambda}_2^\mathrm{T}\frac{\partial\mathbf{K}_\mathrm{d}}{\partial\boldsymbol{\rho}}\mathbf{u}_\mathrm{d} + \left[-\boldsymbol{\lambda}_1^\mathrm{T}\mathbf{K} - \boldsymbol{\lambda}_2^\mathrm{T}\frac{\partial\mathbf{K}_\mathrm{d}}{\partial\mathbf{u}}\mathbf{u}_\mathrm{d}\right]\frac{\mathrm{d}\mathbf{u}}{\mathrm{d}\boldsymbol{\rho}} + \left[\mathbf{f}_\mathrm{os}^\mathrm{T} - \boldsymbol{\lambda}_2^\mathrm{T}\mathbf{K}_\mathrm{d}(\mathbf{u})\right]\frac{\mathrm{d}\mathbf{u}_\mathrm{d}}{\mathrm{d}\boldsymbol{\rho}} \tag{48}$$

To eliminate the implicit derivatives, the terms between square brackets must be equal to zero.

$$-\boldsymbol{\lambda}_1^\mathrm{T}\mathbf{K} - \boldsymbol{\lambda}_2^\mathrm{T}\frac{\partial\mathbf{K}_\mathrm{d}}{\partial\mathbf{u}}\mathbf{u}_\mathrm{d} = 0 \tag{49}$$

$$\mathbf{f}_\mathrm{os}^\mathrm{T} - \boldsymbol{\lambda}_2^\mathrm{T}\mathbf{K}_\mathrm{d}(\mathbf{u}) = 0 \tag{50}$$

This leads to the following expressions for the adjoint terms $\boldsymbol{\lambda}_i$:

$$\boldsymbol{\lambda}_1 = -\mathbf{K}^{-1}\left(\mathbf{u}_\mathrm{d}^\mathrm{T}\frac{\partial\mathbf{K}_\mathrm{d}}{\partial\mathbf{u}}\mathbf{u}_\mathrm{d}\right) \tag{51}$$

$$\boldsymbol{\lambda}_2 = \left[\mathbf{K}_\mathrm{d}(\mathbf{u})\right]^{-1}\mathbf{f}_\mathrm{os} = \mathbf{u}_\mathrm{d} \tag{52}$$

The derivative of the one-step compliance can be reformulated as:

$$\frac{\mathrm{d}C_\mathrm{d}}{\mathrm{d}\boldsymbol{\rho}} = -\boldsymbol{\lambda}_1^\mathrm{T}\frac{\partial\mathbf{K}}{\partial\boldsymbol{\rho}}\mathbf{u} - \mathbf{u}_\mathrm{d}^\mathrm{T}\frac{\partial\mathbf{K}_\mathrm{d}}{\partial\boldsymbol{\rho}}\mathbf{u}_\mathrm{d} \tag{53}$$

DATA AVAILABILITY STATEMENT

The data that support the findings of this study are available from the corresponding author upon reasonable request.

References

1. Bendsøe MP, Kikuchi N. Generating optimal topologies in structural design using a homogenization method. *Computer Methods in Applied Mechanics and Engineering* 1988; 71: 179–224.

2. Duysinx P, Sigmund O. New developments in handling stress constraints in optimal material distribution. In: *7th AIAA/USAF/NASA/ISSMO symposium on multidisciplinary analysis and optimization*; 1998: 4906.

3. Bruggi M. On an alternative approach to stress constraints relaxation in topology optimization. *Structural and Multidisciplinary Optimization* 2008; 36(2): 125–141. doi: 10.1007/s00158-007-0203-6

4. Le C, Norato J, Bruns T, Ha C, Tortorelli D. Stress-based topology optimization for continua. *Structural and Multidisciplinary Optimization* 2010; 41(4): 605–620.

5. Pereira JT, Fancello EA, Barcellos CS. Topology optimization of continuum structures with material failure constraints. *Structural and Multidisciplinary Optimization* 2004; 26(1-2): 50–66.

6. da Silva GA, Beck AT. Reliability-based topology optimization of continuum structures subject to local stress constraints. *Structural and Multidisciplinary Optimization* 2018; 57(6): 2339–2355.

7. da Silva GA, Beck AT, Sigmund O. Stress-constrained topology optimization considering uniform manufacturing uncertainties. *Computer Methods in Applied Mechanics and Engineering* 2019; 344: 512–537.

8. Maute K, Schwarz S, Ramm E. Adaptive topology optimization of elastoplastic structures. *Structural Optimization* 1998; 15(2): 81–91.

9. Russ JB, Waisman H. A novel elastoplastic topology optimization formulation for enhanced failure resistance via local ductile failure constraints and linear buckling analysis. *Computer Methods in Applied Mechanics and Engineering* 2021; 373: 113478.

10. Amir O. A topology optimization procedure for reinforced concrete structures. *Computers & Structures* 2013; 114: 46–58.

11. Amir O, Sigmund O. Reinforcement layout design for concrete structures based on continuum damage and truss topology optimization. *Structural and Multidisciplinary Optimization* 2013; 47(2): 157–174.

12. James KA, Waisman H. Failure mitigation in optimal topology design using a coupled nonlinear continuum damage model. *International Journal for Numerical Methods in Engineering* 2014; 268: 614–631.

13. Noël L. *Level set optimization of bimaterial structures and microstructures considering stress and damage resistance*. PhD thesis. Aerospace and Mechanical Engineering Department, University of Liège, Liège, Belgium; 2016.

14. Da D, Yvonnet J, Xia L, Li G. Topology optimization of particle-matrix composites for optimal fracture resistance taking into account interfacial damage. *International Journal for Numerical Methods in Engineering* 2018; 115(5): 604–626.

15. Peerlings RHJ, de Borst R, Brekelmans WAM, Geers MGD. Gradient-enhanced damage modelling of concrete fracture. *Mechanics of Cohesive-frictional Materials: An International Journal on Experiments, Modelling and Computation of Materials and Structures* 1998; 3(4): 323–342.

16. De Vree JHP, Brekelmans WAM, Van Gils MAJ. Comparison of nonlocal approaches in continuum damage mechanics. *Computers & Structures* 1995; 55(4): 581–588.

17. Kreisselmeier G, Steinhauser R. Systematic Control Design by Optimizing a Vector Performance Index. *IFAC Proceedings Volumes* 1979; 12(7): 113 - 117. IFAC Symposium on computer Aided Design of Control Systems, Zurich, Switzerland, 29-31 Augustdoi: https://doi.org/10.1016/S1474-6670(17)65584-8

18. Peerlings RHJ, de Borst R, Brekelmans WAM, De Vree JHP. Gradient enhanced damage for quasi-brittle materials. *International Journal for Numerical Methods in Engineering* 1996; 39(19): 3391–3403.

19. Bažant ZP, Pijaudier-Cabot G. Nonlocal continuum damage, localization instability and convergence. *Journal of Applied Mechanics* 1988; 55(2): 287–293.

20. Batoz JL, Dhatt G. Incremental displacement algorithms for nonlinear problems. *International Journal for Numerical Methods in Engineering* 1979; 14(8): 1262-1267. doi: 10.1002/nme.1620140811

21. Wang F, Lazarov BS, Sigmund O. On projection methods, convergence and robust formulations in topology optimization. *Structural and Multidisciplinary Optimization* 2011; 43(6): 767-784.

22. Sigmund O, Petersson J. Numerical instabilities in topology optimization: A survey on procedures dealing with checkerboards, mesh-dependencies and local minima. *Structural Optimization* 1998; 16(1): 68–75.

23. Díaz AR, Sigmund O. Checkerboard Patterns in Layout Optimization. *Structural Optimization* 1995; 10(1): 40–45.

24. Lazarov BS, Sigmund O. Filters in topology optimization based on Helmholtz-type differential equations. *International Journal for Numerical Methods in Engineering* 2011; 86(6): 765–781.

25. Bendsøe MP, Sigmund O. *Topology optimization: theory, methods and applications*. Berlin: Springer . 2003.

26. Svanberg K. The Method of Moving Asymptotes - a New Method for Structural Optimization. *International Journal for Numerical Methods in Engineering* 1987; 24(2): 359–373.

27. Sigmund O. Morphology-based black and white filters for topology optimization. *Structural and Multidisciplinary Optimization* 2007; 33(4–5): 401–424.

How to cite this article: Barbier T, Shakour E, Sigmund O, Lombaert G, and Schevenels M. (2021), Topology optimization of damage-resistant structures with a predefined load-bearing capacity, *Int J Numer Meth Engng.*, *xxxx;xx:x–x*.